

# Spectral Efficiency of Adaptive Coded Modulation in Urban Microcellular Networks

Kjell J. Hole, *Member, IEEE*, and Geir E. Øien

**Abstract**—This tutorial paper describes a general adaptive coded modulation scheme for airlinks in urban wireless networks. Each airlink is degraded by shadowed Nakagami multipath fading, interference from other airlinks, and signal path loss. An instance of the adaptive coding scheme utilizes a set of trellis codes originally designed for additive white Gaussian noise channels. A model of the worst and best case interference configurations of a fully loaded network is developed to approximate the average link spectral efficiency (ALSE) of an arbitrary instance of the coding scheme. It is then shown why the ALSE of the adaptive coding scheme is larger than the fixed link spectral efficiency of a traditional nonadaptive coding scheme. Moreover, the ALSE approximation is modified to approximate the average area spectral efficiency (AASE) of the network, and how the cellular layout influences the AASE is shown.

**Index Terms**—Adaptive coded modulation, cellular networks, Nakagami multipath fading, spectral efficiency.

## I. INTRODUCTION

MANY authors [1]–[16] have contributed to the development of adaptive coded modulation schemes for single-user channels with frequency-flat slowly varying multipath fading. A particular instance of such an adaptive coding scheme utilizes a set of trellis codes originally designed for additive white Gaussian noise (AWGN) channels. A feedback channel between the transmitter and the receiver makes it possible to transmit at high information rates under favorable channel conditions and respond to channel degradation through a smooth reduction of the information rate. The adaptive coding schemes described in [8], [9], and [14] utilize sets of two-dimensional trellis codes [17]–[19]. In addition to two-dimensional codes, the adaptive coding scheme in [16] may also utilize sets of multidimensional trellis codes, i.e., in practice codes with dimensions of four, six, and eight [20]–[23]. Multidimensional trellis codes are of particular interest to designers of communication systems since some multidimensional codes offer a significantly better performance/complexity tradeoff than two-dimensional codes [21], [24].

In this tutorial paper, we employ the adaptive coded modulation scheme of [16] in outdoor wireless networks for urban centers with nearly equal-size street blocks. Such networks

are often called Manhattan networks. Our Manhattan network model consists of uniformly spaced quadratic cells, denoted *microcells*, because their width is assumed to be no more than 1 km. Each cell has a base station (BS) located at its center. The city streets form a regular pattern with a BS in the middle of every intersection. A vehicle-mounted or portable mobile station (MS) may be positioned anywhere in the streets but not inside any of the buildings. Since urban centers typically contain a large number of active MSs, we assume that the cellular network model is fully loaded, i.e., the cells' communication links are all fully used.

When an MS accesses the network it is assigned two different carriers: one for the forward (BS-to-MS) link and one for the reverse (MS-to-BS) link. Since the battery power of the MS is severely limited compared to the available power at the stationary BS, the ability of the MS to transmit data over the reverse link is much less than the ability of the BS to transmit over the forward link. We therefore concentrate our study on the reverse links of fully loaded networks. The networks we study use frequency-division multiple access (FDMA) or time-division multiple access (TDMA). The link signals are degraded by *random* Nakagami multipath fading (NMF), shadowing, and interference from other links. There is also a *deterministic* signal power loss, or *path loss*, due to the decay in the intensity of a propagating radio wave.

We may define the information rate of a single reverse link as the number of received information bits per second at the BS for a given transmit power and output bit error rate (BER). For an adaptively coded reverse link where the information rate, denoted by  $R$  [bits/s], is allowed to vary with the changing *carrier-to-interference power ratio* (CIR), the average information rate  $\langle R \rangle$  [bits/s] is obtained by averaging  $R$  over all different CIRs.

Let  $U$  be the number of serviced MSs in a cell of a fully loaded network, and let  $W$  [Hz] be the total bandwidth of the  $U$  reverse links. Assume that all MSs use the same transmit power. It is then natural to define the *average link spectral efficiency* (ALSE) of a single reverse link as  $\langle R \rangle / B$  [bits/s/Hz], where  $B = W/U$  [Hz], for both FDMA and TDMA. The first goal of this paper is to approximate the ALSE of the reverse links in a fully loaded Manhattan network when all links utilize the same instance of the adaptive coding scheme introduced in [16].

Using results in [25]–[30], we develop an idealized model of a fully loaded Manhattan network in Section II. The impairments of the reverse links in a cell are modeled for the worst and best case configurations of the interfering MSs in neighboring cells. It is shown that the instantaneous received CIR at the BS

Manuscript received March 30, 2000; revised October 2, 2000.

K. J. Hole is with the Department of Informatics, University of Bergen, Bergen N-5020 Norway (e-mail: Kjell.Hole@ii.uib.no).

G. E. Øien is with the Department of Telecommunications, Norwegian University of Science and Technology, Trondheim N-7491, Norway (e-mail: Geir.Oien@tele.ntnu.no).

Publisher Item Identifier S 0018-9545(01)01228-2.

is approximately log-normally distributed. The adaptive coding scheme in [16] is also described, and it is shown how the scheme fits into the network model.

The log-normal approximation of the CIR distribution is used in Section III to develop a new technique to approximate the ALSE. Because of the signal path loss, the obtained expression approximating the link ALSE is a function of the distance between the transmitting MS and the receiving BS.

The second aim of this paper is to compare adaptive coded modulation to nonadaptive coded modulation. The careful network modeling carried out in Section II allows us to show, in Section IV, that all spectrally efficient coding schemes for Manhattan networks must be able to operate over a large range of CIR values. This observation is then used to show why it is possible to obtain a larger spectral efficiency with an adaptive coding scheme than with a nonadaptive coding scheme when the schemes are based on Viterbi decoding of traditional trellis codes. It is likely that iterative decoding techniques [31]–[35] will enable us to further increase the spectral efficiency of both adaptive and nonadaptive schemes. For nearly maximal spectral efficiencies, we explain why an adaptive scheme will have a much shorter decoding delay than a nonadaptive scheme.

To determine the cellular layout of a Manhattan network, the available frequency spectrum is first divided over one *cluster* of adjacent cells such that the individual cells in the cluster utilize different sets of carrier frequencies. The complete network is then obtained by deploying many copies of the cell cluster. Let  $K$  be the number of cells in a cluster, and let  $A$  [m<sup>2</sup>] be the area of a single cell. The *average area spectral efficiency* (AASE) is then given by  $(\langle R \rangle / B) / (K \cdot A)$  [bits/s]/[Hz·m<sup>2</sup>]. The AASE provides a measure of the spectral efficiency of the complete network. Our last goal is to approximate the AASE and to show how the cellular layout influences the AASE. This is done in Section V. A summary and concluding remarks are given in Section VI.

## II. NETWORK MODEL AND CODING SCHEME

In this section, we show how the adaptive coding scheme described in [16] fits into an idealized model of a microcellular network for urban centers with a high number of slow-moving pedestrians and vehicles.

### A. Model of Fully Loaded Microcellular Network

A model of an urban center with a microcellular network is depicted in Fig. 1. It contains tall buildings of equal size. The streets between the buildings form a regular pattern with evenly spaced intersections. The BSs are deployed in the middle of the intersections, and the MSs are randomly positioned in the streets.

Recall that we study the MS-to-BS links. It is assumed that each MS has one omnidirectional transmit antenna and that each BS has one omnidirectional receive antenna. Let the height of an antenna be the vertical distance from the ground to the antenna element itself. Since the transmit-antenna height of each MS and the receive-antenna height of each BS are assumed to be much

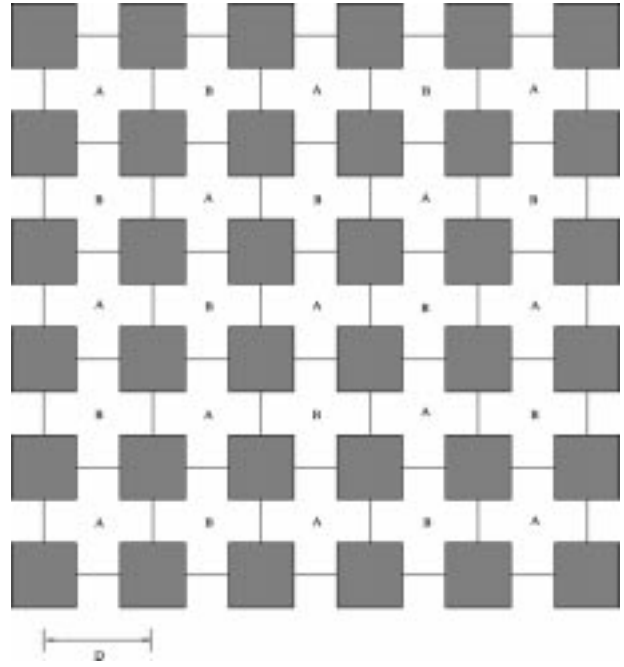


Fig. 1. Idealized model of urban microcellular network consisting of square cells with length  $D$ . The dark squares represent tall buildings, and the space between the dark squares represent streets.

shorter than the buildings, but taller than the vehicular traffic, the buildings act as waveguides channeling signal energy along the street corridors [25], [26].

The microcells are squares with sides, denoted by  $D$  [m], on the order of 400 m to 1 km (see Fig. 1). Each microcell is divided into two parts, a “cross shape” service area defined by the area of the two streets in the cell, and a nonservice area defined by the area of the four buildings intersecting the cell [26].

The same set of carrier frequencies is used in each of the cells labeled A in Fig. 1. A different set of carrier frequencies is used for all cells labeled B. The reuse of a carrier frequency in different cells causes *cochannel interference*, while the use of different carrier frequencies causes *interchannel interference*. Thus, there will be cochannel interference between cells with the same label in Fig. 1 and interchannel interference between cells with different labels. We ignore all interchannel interference, assuming that all carrier frequencies are so far apart that the interchannel interference power is much smaller than the cochannel interference power.

In addition to the cochannel interference, a radio signal from an MS to a BS is also degraded by NMF, shadowing, and AWGN. Both NMF and shadowing are due to randomly delayed reflections, diffraction, and scattering of the radio signal. NMF manifests itself as large changes in the phase and amplitude of the received signal at a BS. The mean of the received signal varies slowly over time because of shadowing. NMF varies fast relative to shadowing but slow compared to the (modulation) symbol rate. We assume that NMF remains nearly constant over hundreds of symbols. AWGN will be ignored for now since its power is usually very small relative to the cochannel interference power in microcellular networks [25].

Pilot symbols are sent repeatedly over the MS-to-BS link to ensure that the time-varying amplitude and phase of the radio signal can be reliably estimated at the BS [36], [37].<sup>1</sup> In the model, the phase estimate is used to fully compensate for phase variation, i.e., we assume coherent detection. Denoting the transmitted complex baseband signal at time  $t \in \{1, 2, \dots\}$  by  $s(t)$ , the coherently demodulated baseband signal is equal to  $z(t) = \alpha(t)s(t)$  where  $\alpha(t)$  is the multiplicative fading envelope (or channel gain) with a Nakagami distribution [28, p. 48], [38]. Observe that  $\alpha(t)$  is real-valued due to the assumption of coherent detection. For simplicity, we will ignore the time reference  $t$  in the remainder of the paper and refer to  $z$ ,  $\alpha$ , and  $s$ .

Let  $S = E[s^2]$  [W] denote the constant transmit power of an MS, where  $E[\cdot]$  is the expectation operator. The instantaneous received power is given by  $P = \alpha^2 S$  [W] with mean denoted by  $E[P] = E[\alpha^2] \cdot S = \Omega$ . Note that  $E[\alpha^2]$ , and therefore  $\Omega$ , varies slowly over time due to shadowing. In fact, the mean measured in decibels,  $10 \log_{10} \Omega$ , may be modeled as a continuous random variable with a normal distribution [28, p. 88]. Using a transformation of random variables, it follows that the random power mean  $\Omega$  has a log-normal probability density function (pdf)

$$p(\Omega) = \frac{\xi}{\sigma_\Omega \Omega \sqrt{2\pi}} \exp\left(-\frac{[10 \log_{10} \Omega - \mu_\Omega(r)]^2}{2\sigma_\Omega^2}\right), \quad \Omega \geq 0 \quad (1)$$

where  $\xi = 10/\ln(10) \approx 4.3429$  and  $\mu_\Omega(r)$  [dB] and  $\sigma_\Omega$  [dB] are the mean and standard deviation of  $10 \log_{10} \Omega$ , respectively. The standard deviation  $\sigma_\Omega$  actually observed in microcells varies between 4 and 13 dB [28, p. 88].

The mean  $\mu_\Omega(r)$  is a deterministic function of the distance  $r$  [m] between the MS and BS. To determine  $\mu_\Omega(r)$ , we first note that any radio signal suffers a deterministic power loss due to the decay in the intensity of a propagating radio wave. We then observe that the placement of a BS in the middle of every intersection in Fig. 1 ensures that there is a line-of-sight (LOS) signal path between an MS in a cell and the cell's BS.<sup>2</sup> The *two-slope* path loss model for microcells with LOS coverage may therefore be used to determine  $\mu_\Omega(r)$  [29], [30]. According to the two-slope model, the mean is given by

$$\mu_\Omega(r) = 10 \log_{10} \left( \frac{F}{r^c(1+r/g)^d} S \right) \text{ [dB]} \quad (2)$$

where  $F$  is a constant,  $c \approx 2$  is the basic path loss exponent, and  $2 \leq d \leq 6$  is the additional path loss exponent. The parameter

$g$  [m] is the *break point* (or turning point) of the path loss curve equal to  $g = (4h_{\text{MS}}h_{\text{BS}})/\lambda$ , where  $h_{\text{MS}}$  [m] is the height of the MS antenna,  $h_{\text{BS}}$  [m] is the height of the BS antenna, and  $\lambda$  [m] is the wavelength of the carrier frequency. Typical antenna heights for microcells are  $h_{\text{MS}} = 2$  m and  $h_{\text{BS}} = 10$  m [30]. The corresponding break points for 900-MHz systems and 2-GHz systems are  $g \approx 240.3$  m and  $g \approx 533$  m, respectively.

The Nakagami pdf of the channel gain  $\alpha$  is controlled by the Nakagami fading parameter  $m$ , a real number  $m \geq 1/2$  [28, p. 48], [38]. We assume that  $m$  is a positive integer. The Nakagami distribution represents a wide range of multipath fading channels via different integer values of the parameter  $m$ . When  $m = 1$ , the pdf is the Rayleigh pdf and the radio signal does not have a direct LOS component. For  $m = 2, 3, \dots$ , the Nakagami distribution closely approximates the Rice distribution used when the signal has a LOS component [28, p. 48]. As  $m$  increases, the LOS component becomes gradually stronger. Since we have LOS coverage in our model,  $m \geq 2$  here.

It is not difficult to see that the instantaneous received signal power  $P = \alpha^2 S$  conditioned on the mean  $\Omega (= E[P] = E[\alpha^2] \cdot S)$  has a gamma distribution when  $\alpha$  has a Nakagami distribution [28, p. 49]. Since the mean of the signal power  $\Omega$  has a log-normal distribution due to shadowing, the instantaneous received power  $P$  has a composite *Gamma-log-normal* distribution. The pdf of this composite distribution is obtained by integrating the pdf for the gamma distributed power  $P$  conditioned on  $\Omega$  over the pdf of the log-normally distributed mean signal power  $\Omega$ . The resulting Gamma-log-normal pdf is given by

$$p(P) = \int_0^\infty \left(\frac{m}{\Omega}\right)^m \frac{P^{m-1}}{\Gamma(m)} \exp\left(-m\frac{P}{\Omega}\right) \cdot \frac{\xi}{\sigma_\Omega \Omega \sqrt{2\pi}} \exp\left(-\frac{[10 \log_{10} \Omega - \mu_\Omega(r)]^2}{2\sigma_\Omega^2}\right) d\Omega \quad (3)$$

where the gamma function  $\Gamma(m) = (m-1)!$  [39, (8.339.1), p. 947] when the Nakagami fading parameter  $m$  is a positive integer.

It is shown in [28, Appendix 2B] that the composite Gamma-log-normal pdf in (3) can be accurately approximated by the log-normal pdf in (1) if  $P$  is substituted for  $\Omega$  and the logarithmic mean  $\mu_\Omega(r)$  and variance  $\sigma_\Omega^2$  are replaced by

$$\begin{aligned} \mu_P(r) &= E[10 \log_{10} P] \\ &= \xi [\psi(m) - \ln(m)] + \mu_\Omega(r) \text{ [dB]} \\ \sigma_P^2 &= E[(10 \log_{10} P)^2] - [\mu_P(r)]^2 \\ &= \xi^2 \zeta(2, m) + \sigma_\Omega^2 \text{ [dB]}. \end{aligned} \quad (4)$$

Here,  $\psi(m)$  is Euler's psi function defined by [39, eq. (8.365.4), p. 954]

$$\psi(m) = -C + \sum_{k=1}^{m-1} \frac{1}{k}$$

<sup>1</sup>The overhead bandwidth associated with the pilot symbols is ignored in this paper.

<sup>2</sup>In fact, if we assume that the network in Fig. 1 contains infinitely many cells, then any MS has LOS signal paths to infinitely many BSs.

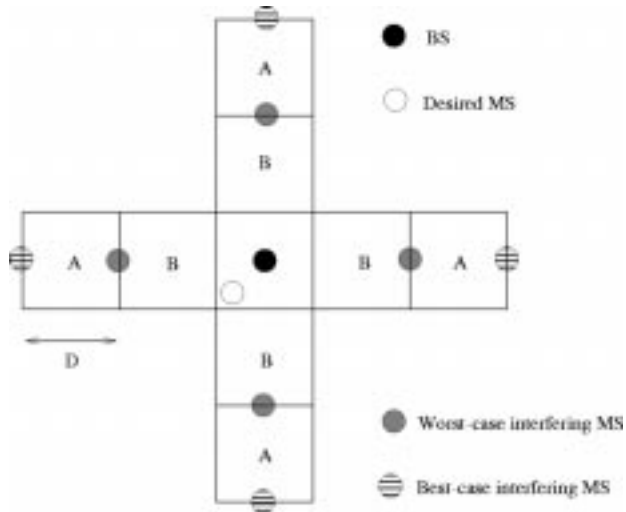


Fig. 2. Worst and best case cochannel interference configurations.

where  $C \approx 0.5772$  is Euler's constant and  $\zeta(\cdot)$  is Riemann's zeta function<sup>3</sup> given by [39, eq. (9.521.1), p. 1101]

$$\zeta(z, n) = \sum_{j=0}^{\infty} \frac{1}{(n+j)^z}, \quad z > 1, n \neq 0, -1, -2, \dots$$

We study a fully loaded Manhattan network with  $U$  serviced MSs in each microcell. Consider the link between an arbitrary transmitting MS, called the *desired MS*, and its BS. In the street microcell deployment in Fig. 1, the effect of non-LOS cochannel interferers on the link performance can be neglected in deference to the dominant effect of the LOS cochannel interferers [28, p. 486]. Also, due to the path loss, we only need to consider the LOS cochannel interferers in the first dominant tier of the interfering cells. Since we assume that the BS has an omnidirectional receive antenna, the worst case (−) and best case (+) interference configurations, depicted in Fig. 2, are given by four MSs, which are either all in distance  $2D - D/2$  [m] or  $2D + D/2$  [m] from the BS for  $D$  [m] equal to the width of the square cells.

Implicitly, we have assumed that both the desired MS and the interfering MSs in Fig. 2 transmit at all times. To see that this assumption is valid both for TDMA and FDMA, we first concentrate on the desired MS. If FDMA is utilized, then the desired MS does indeed transmit continuously using a fraction  $B = W/U$  of the bandwidth. On the other hand, if TDMA is utilized, then the overall signaling rate is increased by a factor of  $U$  relative to FDMA. However, only one MS transmits at a given time, with each MS using every  $U$ th time slot. This yields the same overall bandwidth and same number of bits per second as transmitting at all times using bandwidth  $B$ .

Next, we consider the interfering MSs. Despite the fact that each of the four neighboring cells contains  $U$  active MSs, we have included only one interfering MS in each of the four neighboring cells in Fig. 2. To see why, we note that for both the worst and best case interference scenarios, all  $U$  active MSs in a neighboring cell are positioned in the same

<sup>3</sup>This function is also called the Hurwitz zeta function or the generalized Riemann zeta function [40, p. 75].

TABLE I  
VALUES OF  $a_n$  AND  $b_n$  USED TO ESTIMATE THE BER (12) OF CODES IN CODEC AND THE THRESHOLD VALUES FOR THE FADING REGIONS

$n$	$M_n$	$a_n$	$b_n$	$\gamma_n$ [dB]
1	4	896.0704	10.7367	7.1
2	8	404.4353	6.8043	11.8
3	16	996.5492	8.7345	14.0
4	32	443.1272	8.2282	17.0
5	64	296.6007	7.9270	20.1
6	128	327.4874	8.2036	23.0
7	256	404.2837	7.8824	26.2
8	512	310.5283	8.2425	29.0

distance  $2D \mp D/2$  from the desired MS's BS. If TDMA is used, only the MS transmitting in the same time slot as the desired MS creates interference. This is the same as having one MS in distance  $2D \mp D/2$  transmitting continuously using a fraction  $B$  of the total bandwidth.

When FDMA is used, all  $U$  interfering MSs transmit at all times, each using the bandwidth  $B$  but at different carrier frequencies. Since we ignore interchannel interference, only the MS transmitting on the same carrier frequency as the desired MS creates interference. Consequently, we may assume that both the desired MS and the four interfering MSs transmit constantly using bandwidth  $B$ .

In the following, we denote the instantaneous received power from the desired MS at the BS by  $P(r)$  [W]. From (2) and (4), the power mean  $\mu_P(r)$  depends on the distance  $r$  between the MS and BS. Let  $S_i(2D \mp D/2)$  [W] denote the received power from the  $i$ th interfering MS at distance  $2D \mp D/2$  from the desired MS's BS. The instantaneous received CIR  $\gamma$  at the BS for the worst and best case interference configurations is given by the random variable

$$\gamma = \frac{P(r)}{\sum_{i=1}^4 S_i(2D \mp D/2)}. \quad (5)$$

As seen from (5), it is assumed that the cochannel interfering signals add up incoherently (i.e., in power) since this leads to a more realistic assessment of the cochannel interference. The received powers  $S_i(2D \mp D/2)$  from the interfering MSs are each approximately log-normally distributed, just like  $P(r)$ . We may assume that these received powers are statistically independent because, for both interference configurations, all interfering MSs are far apart. Also, since all the interfering MSs are equally far away from the BS for each of the configurations, we may assume that the powers  $S_i(\cdot)$  have equal mean and variance

$$\begin{aligned} \mu_{I, \mp} &= \xi[\psi(m_I) - \ln(m_I)] + \mu_{\Omega}(2D \mp D/2) \text{ [dB]} \\ \sigma_I^2 &= \xi^2 \zeta(2, m_I) + \sigma_{\Omega}^2 \text{ [dB]} \end{aligned} \quad (6)$$

where  $m_I$  is the Nakagami parameter for the interferers, restricted to integer values in this paper.

The distribution of the sum of the four independent identically distributed log-normally distributed random variables  $S_I = \sum_{i=1}^4 S_i(2D \mp D/2)$  in (5) may be approximated up to

second-order moments by yet another log-normal distribution [28, Sec. 3.1]. Using the *Fenton–Wilkinson method* [28, Sec. 3.1.1] (see also [27]), it is possible to show that this approximated log-normal pdf of  $S_I$  has logarithmic mean and variance

$$\begin{aligned}\mu_{S_I, \mp} &= \mu_{I, \mp} + \xi \ln(4) + \frac{\sigma_I^2}{2\xi} - \frac{\xi}{2} \ln\left(\frac{3 + e^{\sigma_I^2/\xi^2}}{4}\right) \text{ [dB]} \\ \sigma_{S_I}^2 &= \xi^2 \ln\left(\frac{3 + e^{\sigma_I^2/\xi^2}}{4}\right) \text{ [dB]}.\end{aligned}\quad (7)$$

Since the numerator and denominator of (5) are both approximately log-normally distributed, it follows that the pdf of the CIR  $\gamma$ , conditioned on the position  $r$  of the desired MS, can again be approximated by a log-normal pdf

$$p(\gamma|r) = \frac{\xi}{\sigma_\gamma \gamma \sqrt{2\pi}} \exp\left(-\frac{[10\log_{10}\gamma - \mu_{\gamma, \mp}(r)]^2}{2\sigma_\gamma^2}\right), \quad \gamma \geq 0 \quad (8)$$

whose logarithmic mean and variance are

$$\begin{aligned}\mu_{\gamma, \mp}(r) &= \mu_P(r) - \mu_{S_I, \mp} \text{ [dB]} \\ \sigma_\gamma^2 &= \sigma_P^2 + \sigma_{S_I}^2 \text{ [dB]}.\end{aligned}\quad (9)$$

We may calculate the mean and variance in (9) by combining expressions. From (2), (4), (6), and (7), we have

$$\begin{aligned}\mu_{\gamma, \mp}(r) &= \xi \ln\left(\left[\frac{2D \mp D/2}{r}\right]^c \left[\frac{g + 2D \mp D/2}{g+r}\right]^d\right) \\ &\quad + \frac{\xi}{2} \ln\left(\frac{3 + e^{\sigma_I^2/\xi^2}}{4}\right) \\ &\quad + \xi \left[\psi(m) - \psi(m_I) - \ln\left(\frac{m}{m_I}\right)\right] \\ &\quad - \xi \ln(4) - \frac{\sigma_I^2}{2\xi} \text{ [dB]}\end{aligned}\quad (10)$$

and from (4) and (7), we have

$$\begin{aligned}\sigma_\gamma^2 &= \xi^2 \left[ \zeta(2, m) + \ln\left(\frac{3 + e^{\sigma_I^2/\xi^2}}{4}\right) \right] \\ &\quad + \sigma_\Omega^2 \text{ [dB]}\end{aligned}\quad (11)$$

where  $\sigma_I^2$  is defined by (6). Note that the third term on the right-hand side of (10) disappears when  $m = m_I$ . Observe also that the constant  $F$  in the two-slope model (2) and the constant transmit power  $S$  of the MSs are not contained in (10) due to cancellation during the calculation of the expression. The cancellation of the transmit power  $S$  depends on the fact that all MSs use the same transmit power.

### B. Adaptive Coding Scheme

In this section, we describe a general adaptive coding scheme, first introduced in [16], for the MS-to-BS links in a Manhattan network. We start with an overview of the assumptions on which the coding scheme is based.

To obtain high spectral efficiency on all links in a cellular network, the information rate of each link should be adapted according to the instantaneous received CIR  $\gamma$  [27]. We assume that the fluctuations in  $\gamma$  are tracked perfectly by the BS receiver. A decision device in the BS utilizes the instantaneous received CIR to select an appropriate information rate by choosing a code among a set of  $2L$ -dimensional ( $2L$ -D) trellis codes for  $L \in \{1, 2, 3, \dots\}$ . The decision device then informs the MS about its decision via the BS-to-MS link. The  $2L$ -D trellis codes should in practice be generated by the same encoder and decoded by the same Viterbi decoder. We assume that the trellis codes are implemented by a variable-rate encoder and decoder (codec) in such a way that it is possible to change rate at any time [8], [9], [16].

For satisfactory operation of an MS-to-BS link, both the variable-rate encoder and the variable-rate Viterbi decoder must use the same code at any instant. An efficient error control scheme is therefore needed on the feedback (BS-to-MS) link to insure near error-free signaling from the BS to the MS. We simply assume that the feedback link is noiseless.

The propagation delay in the feedback link may reduce the achievable average spectral efficiency for a given output BER at the BS when the instantaneous received CIR  $\gamma$  changes rapidly. We have assumed that  $\gamma$  changes at a rate much slower than the symbol rate, and we therefore ignore the propagation delay in this paper.

We now describe the details of the coding scheme. The instantaneous received CIR  $\gamma$  is quantized and one  $2L$ -D trellis code is assigned to each quantization level (or fading region). We define the  $N$  fading regions by the thresholds  $\gamma_1 < \gamma_2 < \dots < \gamma_{N+1}$ . Code  $n$ ,  $n = 1, 2, \dots, N$ , is used when  $\gamma$  falls in region  $n$ , i.e., when  $\gamma_n \leq \gamma < \gamma_{n+1}$ . Fading region 1 represents the smallest values of  $\gamma$  for which information is transmitted. When  $\gamma < \gamma_1$ , no information is sent. Hence, the probability that  $\gamma < \gamma_1$  is called the *outage probability*.

We use  $N$  trellis codes originally designed for AWGN channels. To understand why, we first observe that the width  $\gamma_{n+1} - \gamma_n$  of each fading region goes to zero when the number of fading regions  $N$  goes to infinity. Consequently, for large  $N$ , the received CIR may be approximated by a constant for each fading region, and we may view the shadowed NMF channel at a given time instant as an element in a set of  $N$  (nearly) fading-free channels with different but constant CIRs. Next, we note that the interference, or “noise,” in each channel is mainly caused by the four active MSs in the first ring of interfering cells (see Fig. 2). Since there are only four dominant interferers, the central limit theorem does not apply, and the interference does not necessarily have Gaussian characteristics. However, we still choose to model each channel in the set by an AWGN channel. AWGN reduces the Shannon capacity the most of any additive noise type. In other words, the interpretation of the interfering MSs as AWGN is a worst case noise assumption with respect to the theoretically obtainable maximal ALSE [6], although not necessarily for the performance of one particular coding scheme.

The  $2L$ -D signal constellation for code  $n$  is given by the  $L$ -fold Cartesian product of a two-dimensional (2-D) signal set with  $M_n = 2^{k_n}$  signal points (or symbols). Each time the encoder for code  $n$  receives  $p = L \cdot k_n - 1$  information bits, it

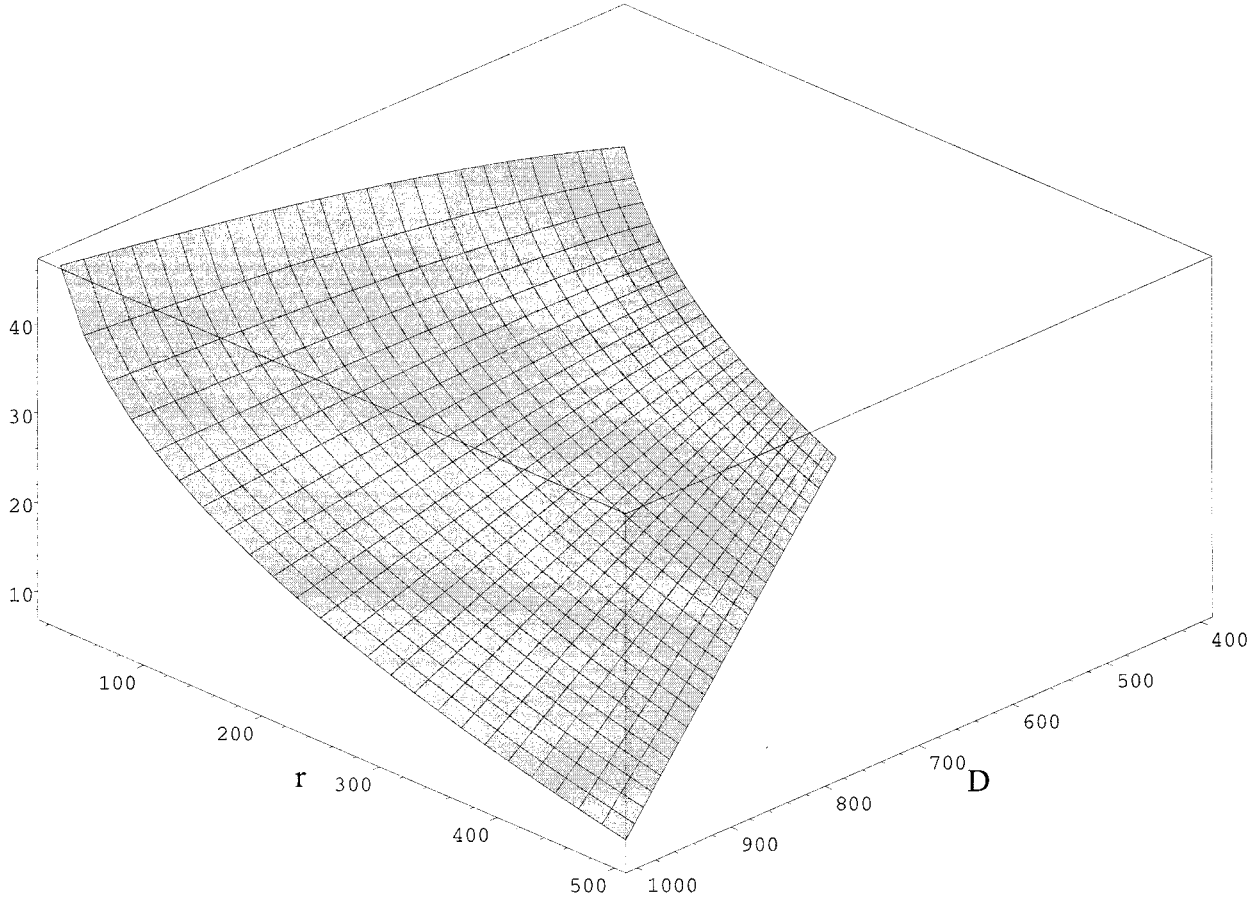


Fig. 3. Mean of instantaneous received CIR [dB] as a function of  $D$  [m] and  $r$  [m], where  $D$  is the length of the square cells and  $r$  is the distance between the desired MS and its BS. (Fully loaded network; worst case interference configuration; target  $\text{BER}_0 = 10^{-3}$ ; two-slope path loss parameters:  $c = d = 2$ ,  $g = 240.3$ ; Nakagami parameters  $m = m_I = 2$ ; standard deviation of shadowed power mean  $\sigma_\Omega = 4$  dB.)

generates  $p + 1 = L \cdot k_n$  coded bits. The coded bits then determine  $L$  transmittable 2-D modulation symbols.

If the time  $T$  between the transmission of two consecutive 2-D symbols is such that there is no intersymbol interference in the samples at the output of the channel, then the information rate for code  $n$  is equal to  $R_n = (\log_2(M_n) - 1/L)/T = (k_n - 1/L)/T$  [bits/s]. Since the Nyquist bandwidth is  $B = 1/T$ , the maximum spectral efficiency for code  $n$  is  $R_n/B = k_n - 1/L$  [bits/s/Hz]. The codes should have spectral efficiencies  $k_n - 1/L$ , which increase with  $\gamma$ , i.e.,  $k_n < k_{n+1}$  for  $n = 1, 2, \dots, N-1$ . This makes it possible to transmit at high spectral efficiencies when there is little or no cochannel interference and shadowed NMF and to reduce the spectral efficiency as the channel impairments increase.

To determine the values of the thresholds  $\gamma_n$ ,  $n = 1, 2, \dots, N$ , it was argued in [16] that the BER of code  $n$  on an AWGN channel can be approximated by an expression of the form

$$\text{BER} \approx a_n \cdot \exp\left(-\frac{b_n \gamma}{M_n}\right) \quad (12)$$

where the constants  $a_n (> 0)$  and  $b_n (> 0)$  depend on the weight distribution of the code. It is possible to obtain good values of

$a_n$  and  $b_n$  by first simulating the codes' BER performance and then curve fitting with the least squares method (see [16] for an example).

The lower threshold  $\gamma_n$  for code  $n$  is equal to the smallest CIR required to achieve a given target BER denoted by  $\text{BER}_0$ . We obtain the following thresholds by assuming equality in (12), substituting  $\gamma_n$  for  $\gamma$  and  $\text{BER}_0$  for BER and inverting the expression with respect to the CIR

$$\begin{aligned} \gamma_n &= (M_n K_n) / b_n, & n = 1, 2, \dots, N \\ \gamma_{N+1} &= \infty \end{aligned} \quad (13)$$

where  $K_n = -\ln(\text{BER}_0/a_n)$ . In practice, we have that  $0 < \text{BER}_0 \leq a_n$  for all  $n$  such that  $K_n \geq 0$  and all thresholds  $\gamma_n \geq 0$ .<sup>4</sup>

### III. GENERAL APPROXIMATION TECHNIQUES

In the following, we develop general techniques to approximate the ALSE and outage probability of all MS-to-BS links in

<sup>4</sup>When the thresholds are chosen according to (13), the instantaneous BER at a BS is smaller than the target  $\text{BER}_0$  for  $\gamma_n < \gamma < \gamma_{n+1}$ . As a result, the average BER at the BS will be below the target  $\text{BER}_0$ . We have made this conservative design choice since in practice propagation delay, estimation errors, etc., will increase the BER.

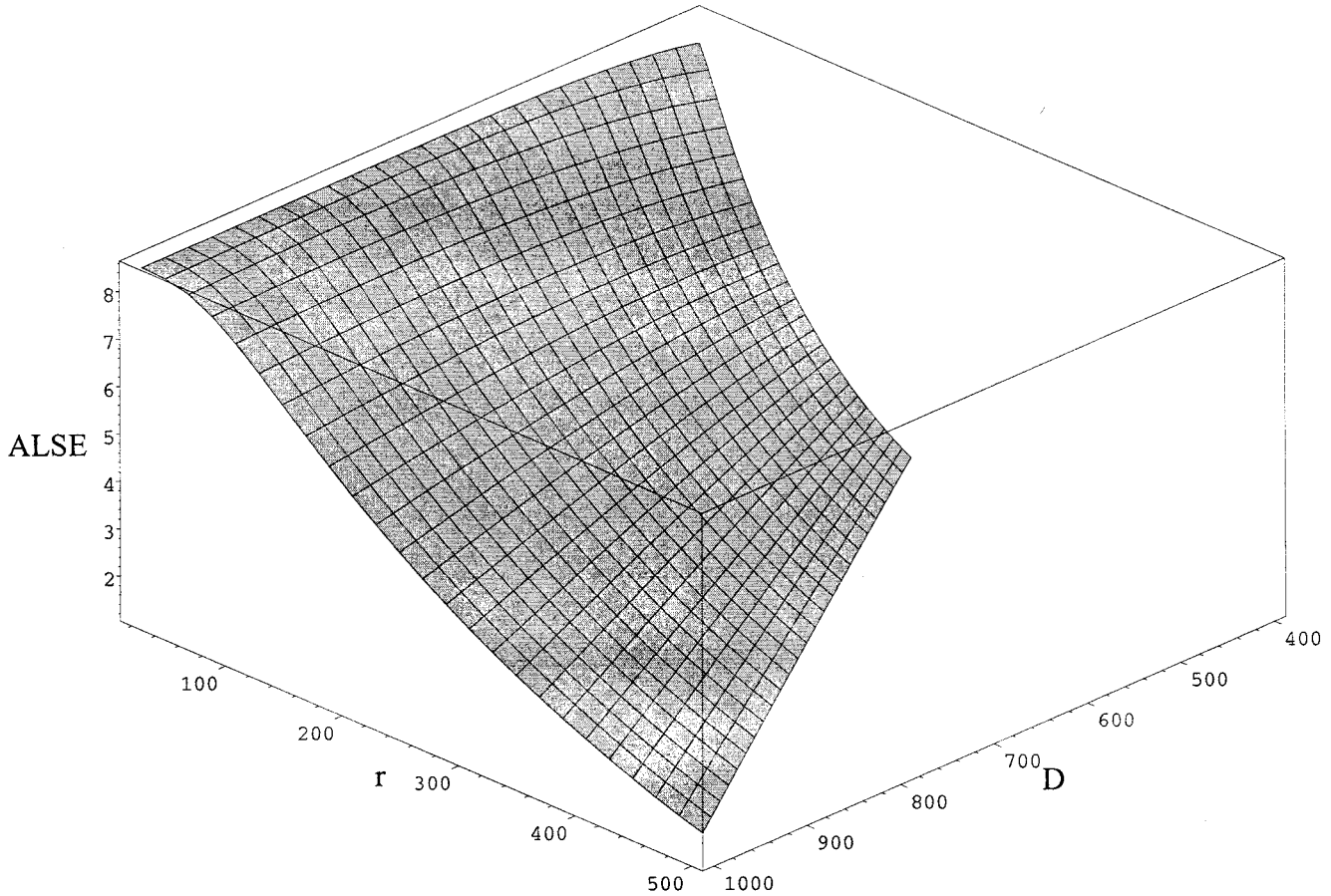


Fig. 4. ALSE [bits/s/Hz] as a function of  $D$  [m] and  $r$  [m], where  $D$  is the length of the square cells and  $r$  is the distance between the desired MS and its BS. (Fully loaded network; worst case interference configuration; target  $\text{BER}_0 = 10^{-3}$ ; two-slope path loss parameters:  $c = d = 2, g = 240.3$ ; Nakagami parameters  $m = m_I = 2$ ; standard deviation of shadowed power mean  $\sigma_\Omega = 4$  dB; code dimension  $2L = 4$ .)

a fully loaded Manhattan network, assuming that all links utilize the same instance of the adaptive coding scheme.

#### A. General Approximation of Spectral Efficiency

Each cell in the network model has  $U$  transmitting MSs using the same transmit power. The bandwidth allocated to each MS is  $B = W/U$  [Hz], where  $W$  was defined to be the total available bandwidth in a cell. Consider an arbitrary MS transmitting information on its MS-to-BS link. For  $r$  [m], the distance between the MS and BS, denoted by  $\langle R|r \rangle$  [bits/s], is the average received information rate from the MS at the BS for a given output BER. The ALSE of the MS-to-BS link, conditioned on  $r$ , is then given by  $\langle R|r \rangle / B$  [bits/s/Hz].

We may approximate the ALSE for the worst and best case interference configurations of a fully loaded network. The expected link spectral efficiency of any instance of the adaptive coding scheme is given by the sum over all  $n$  of the individual codes' spectral efficiencies  $R_n/B = k_n - 1/L$ , each weighted by the probability  $P_{\mp, r}(\gamma_n, \gamma_{n+1})$  that code  $n$  is used, i.e., the CIR  $\gamma$  falls in fading region  $n$

$$\frac{\langle R|r \rangle_{\mp}}{B} = \sum_{n=1}^N (k_n - 1/L) P_{\mp, r}(\gamma_n, \gamma_{n+1}) \text{ [bits/s/Hz]}. \quad (14)$$

The probabilities in (14) are equal to  $P_{\mp, r}(\gamma_n, \gamma_{n+1}) = \int_{\gamma_n}^{\gamma_{n+1}} p(\gamma|r) d\gamma$  where the pdf  $p(\gamma|r)$  is defined by (8) and the thresholds  $\gamma_n$  and  $\gamma_{n+1}$  are given by (13). The subscripts  $\mp$  and  $r$  indicate that the values of the probabilities depend on which of the two interference configurations we consider as well as the distance  $r$  between the MS and the BS.

To calculate  $P_{\mp, r}(\gamma_n, \gamma_{n+1})$ , we need the *signum function*

$$\text{sgn}(x) = \begin{cases} +1, & \text{if } x \geq 0 \\ -1, & \text{if } x < 0 \end{cases}$$

and the *error function*

$$\text{erf}(u) = \frac{2}{\sqrt{\pi}} \int_0^u \exp(-x^2) dx. \quad (16)$$

For any real number  $\beta \geq 0$ , we also need to define the function

$$\chi(\beta) = \begin{cases} \frac{10 \log_{10} \beta - \mu_{\gamma, \mp}(r)}{\sqrt{2} \sigma_\gamma}, & \text{if } \beta > 0 \\ -\infty, & \text{if } \beta = 0. \end{cases} \quad (17)$$

Observe that the extension to  $\beta = 0$  is natural since  $\log_{10} \beta \rightarrow -\infty$  when  $\beta \rightarrow 0^+$ .

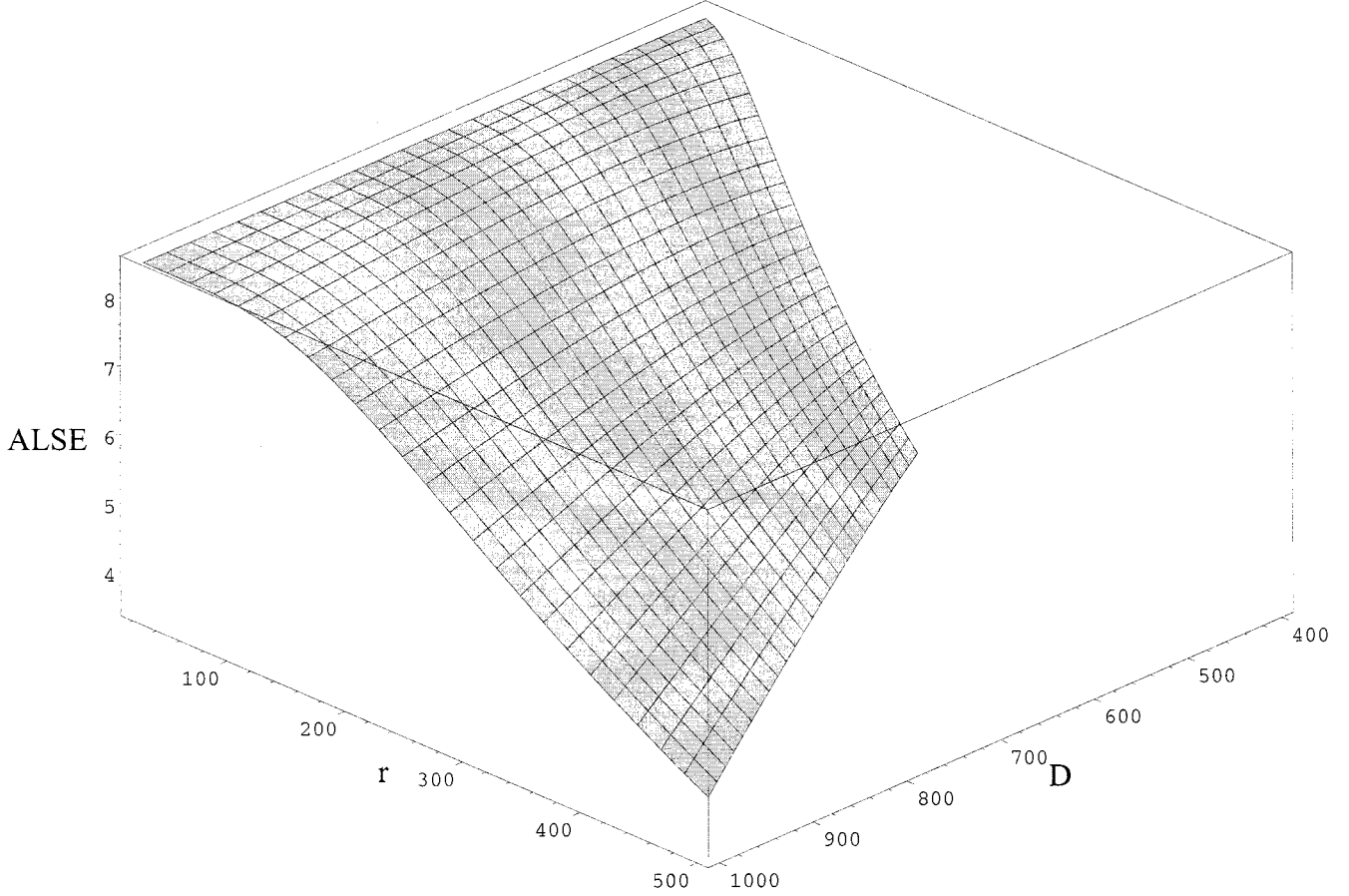


Fig. 5. ALSE [bits/s/Hz] as a function of  $D$  [m] and  $r$  [m], where  $D$  is the length of the square cells and  $r$  is the distance between the desired MS and its BS. (Fully loaded network; best-case interference configuration; target  $\text{BER}_0 = 10^{-3}$ ; two-slope path loss parameters:  $c = d = 2, g = 240.3$ ; Nakagami parameters  $m = m_I = 2$ ; standard deviation of shadowed power mean  $\sigma_\Omega = 4$  dB; code dimension  $2L = 4$ .)

It is shown in an Appendix that

$$P_{\mp, r}(\beta, \infty) = \frac{\text{sgn}(-\chi(\beta)) \cdot \text{erf}(|\chi(\beta)|) + 1}{2}.$$

Since the thresholds  $\gamma_n$  have nonnegative values and

$$P_{\mp, r}(\gamma_n, \gamma_{n+1}) = P_{\mp, r}(\gamma_n, \infty) - P_{\mp, r}(\gamma_{n+1}, \infty)$$

we obtain (18) as shown at the bottom of the page. Note that because  $\chi(0) = -\infty, \chi(\infty) = \infty$ , and  $\text{erf}(\infty) = 1$ , we have  $P_{\mp, r}(0, \infty) = 1$  as we should.

The final expression for the ALSE conditioned on  $r$  is obtained by combining the expressions in (14) and (18). It is of course possible to average the ALSE over all values of  $r$  (see [27]). We do not average over  $r$  in this paper since, as we shall see in Section IV, a good knowledge of the ALSE variations is

needed to determine spectrally efficient trellis codes for Manhattan networks. In fact, such codes will depend on the actual values of  $r$ .

#### B. General Approximation of Outage Probability

An active MS does not transmit any information when the received CIR  $\gamma$  falls below the threshold  $\gamma_1$ . As a result, the MS suffers an outage probability approximated by

$$P_{\text{out}}(\gamma_1) = 1 - P_{\mp, r}(\gamma_1, \infty) = \frac{1 - \text{sgn}(-\chi(\gamma_1)) \cdot \text{erf}(|\chi(\gamma_1)|)}{2}. \quad (19)$$

The outage probability increases with growing threshold value  $\gamma_1 = (M_1 K_1)/b_1$ . Since the value of  $K_1 = -\ln(\text{BER}_0/a_1)$  increases with decreasing target  $\text{BER}_0$ , it follows that the outage probability grows with decreasing target  $\text{BER}_0$ . Hence, there is a tradeoff between wanting a small target BER and a small outage probability.

$$P_{\mp, r}(\gamma_n, \gamma_{n+1}) = \frac{\text{sgn}(-\chi(\gamma_n)) \cdot \text{erf}(|\chi(\gamma_n)|) - \text{sgn}(-\chi(\gamma_{n+1})) \cdot \text{erf}(|\chi(\gamma_{n+1})|)}{2}. \quad (18)$$

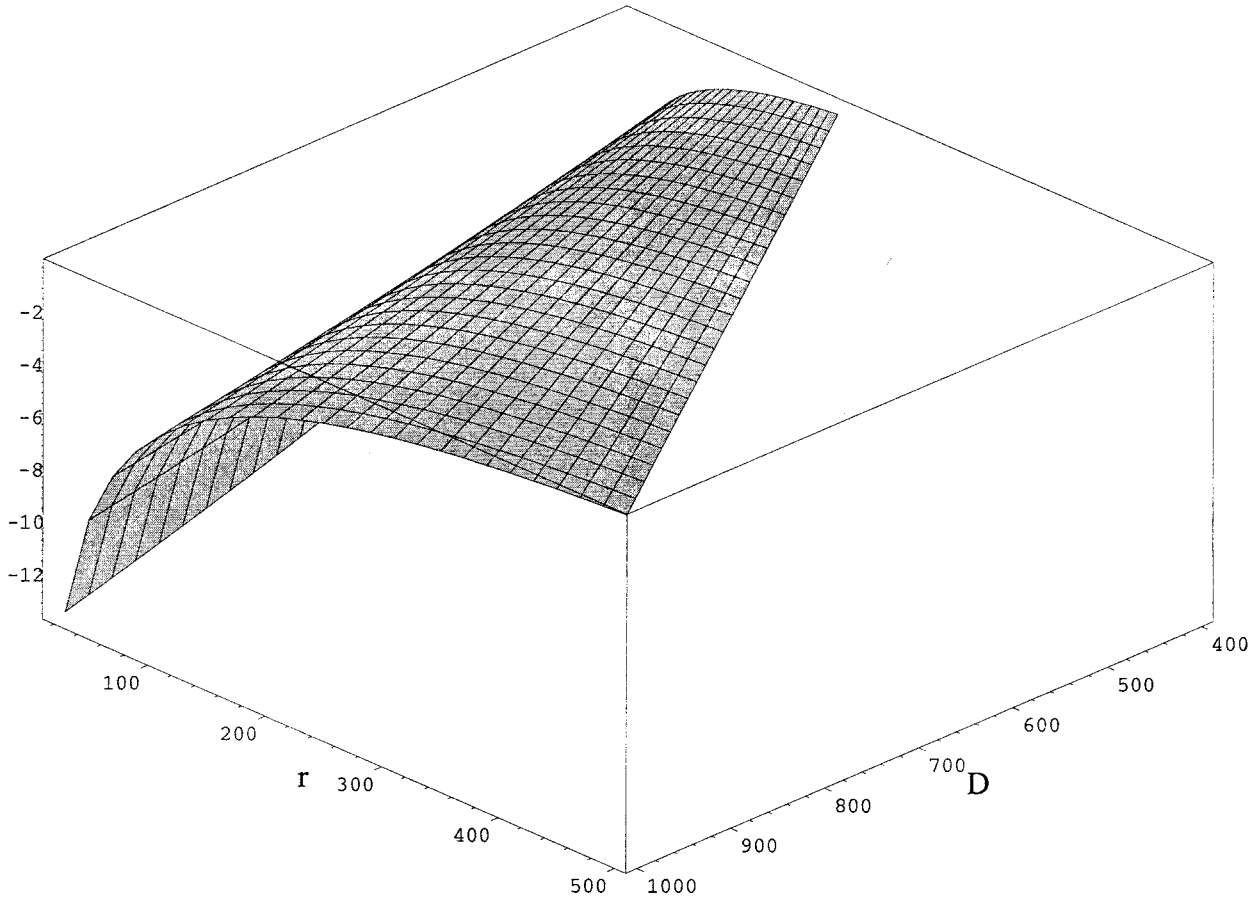


Fig. 6. Base-10 logarithm of outage probability as a function of  $D$  [m] and  $r$  [m], where  $D$  is the length of the square cells and  $r$  is the distance between the desired MS and its BS. (Fully loaded network; worst case interference configuration; target  $\text{BER}_0 = 10^{-3}$ ; two-slope path loss parameters:  $c = d = 2$ ,  $g = 240.3$ ; Nakagami parameters  $m = m_I = 2$ ; standard deviation of shadowed power mean  $\sigma_\Omega = 4$  dB; code dimension  $2L = 4$ .)

### C. Evaluation of Example Codec

As an illustrative example, we approximate the ALSE when identical copies of a particular adaptive codec introduced in [16] are used to encode and decode the information on all MS-to-BS links in a fully loaded Manhattan network.

The adaptive codec considered here utilizes trellis-coded multilevel quadrature amplitude modulation (M-QAM). The codec contains eight four-dimensional (4-D) trellis codes based on eight nested M-QAM signal constellations with  $M_n = 2^{k_n} \in \{4, 8, 16, 32, 64, 128, 256, 512\}$  signal points for  $k_n = n + 1$  and  $n = 1, 2, \dots, 8$  [16, Fig. 1]. At each *even* time instant  $2t$ , the variable-rate encoder receives  $p(2t)$  information bits,  $p(2t) \in \{3, 5, 7, 9, \dots, 17\}$  and generates  $p(2t)+1$  coded bits. The overall encoder contains the rate 2/3 trellis encoder and bit converter but not the 4-D block encoder, depicted in [20, Fig. 6]. The rate 2/3 trellis encoder and bit converter are also used in the International Telecommunications Union's ITU-T V.34 modem standard. [41], [42].<sup>5</sup> The soft decision Viterbi decoder for the code with  $p(2t) = 17$  is used to decode the codes with  $p(2t) < 17$  since these codes are all contained in the  $p(2t) = 17$  code.

<sup>5</sup>The constellation shaping via shell mapping implemented in the V.34 modem was not used in the example codec.

The individual codes' BER performance on an AWGN channel have been simulated for various carrier-to-noise ratios (CNRs) in [16]. Curve fitting with the least squares method was then used to obtain values for the parameters  $a_n$  and  $b_n$  in the BER approximation (12). For convenience, the obtained values are given in Table I.

We choose the target BER at the BS to be  $\text{BER}_0 = 10^{-3}$ . For the  $a_n$  and  $b_n$  values in Table I, we then use (13) to obtain the threshold values  $\gamma_n$  [dB] listed in the right-most column of Table I.

The mean of the instantaneous received CIR  $\gamma$ , defined by (10), is plotted in Fig. 3 for the worst case interference configuration,  $D = 400, \dots, 1000$  m and  $r = 20, \dots, D/2$  m (the values of the other model parameters are given in the figure caption). As is to be expected, for a fixed length  $D$  of the cells, the mean CIR decreases with growing distance  $r$  between the desired MS and its BS. When we keep  $r$  fixed, the mean decreases with shrinking  $D$  since the distance between the BS and the interfering MSs becomes smaller. For fixed  $r = 100$  m, the mean value is 30.2 dB for  $D = 1000$  m, while the mean is only 15.9 dB for  $D = 400$  m.

We plot the ALSE (14) in Fig. 4. For a fixed length  $D$  of the cells, the ALSE decreases with growing distance  $r$  between the desired MS and its BS. When we keep  $r$  fixed, the ALSE decreases with shrinking  $D$ . There are large differences in the

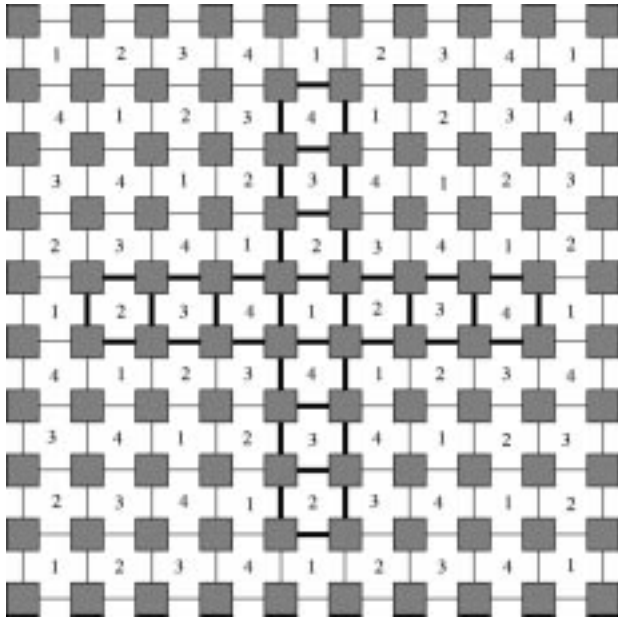


Fig. 7. Idealized model of urban microcellular network with a four-cell reuse pattern and BSs that are deployed in the middle of every intersection. All cells labeled with the same number use the same set of carrier frequencies for the MS-to-BS links. LOS cochannel cells are separated by at least three cells, while there are no reuse constraints on non-LOS cochannel cells.

ALSE values: when  $r = 20$  and  $D = 1000$ , the ALSE has value 8.5; for  $r = 200$  and  $D = 400$ , the ALSE is 1.2.

The ALSE for the best case interference configuration is plotted in Fig. 5. When  $r = 200$  and  $D = 400$ , the ALSE is 3.5, i.e., 2.9 times more than for the worst case interference configuration.

The base-10 logarithm of the outage probability (19) is plotted in Fig. 6 for the worst case interference configuration. For  $r = 20$  and  $D = 1000$ , the probability is  $0.3 \cdot 10^{-13}$ , while for  $r = 200$  and  $D = 400$ , the probability is 0.5.

#### D. More General Manhattan Networks

Let us consider an arbitrary Manhattan network consisting of equally large square cells with sides of length  $D$  [m]. Define the *reuse distance*,  $\mathcal{R}$  [m], to be the minimum distance between two BSs that are within LOS of each other and that use the same set of carrier frequencies for the MS-to-BS links. The Manhattan network in Fig. 1 has a two-cell frequency reuse pattern resulting in a reuse distance of  $\mathcal{R} = 2D$ .

Fig. 7 depicts a Manhattan network with a four-cell reuse pattern. The LOS cochannel cells are separated by at least three cells, giving a reuse distance of  $\mathcal{R} = 4D$ . The worst and best case interference configurations are depicted in Fig. 8. All worst case ( $-$ ) and best case ( $+$ ) MSs are a distance  $\mathcal{R} \mp D/2$  from the BS. In fact, this expression determines the distances from the BS for any reuse distance  $\mathcal{R}$ . Hence, to use our approximation techniques for any Manhattan network with equally large square cells, we only need to substitute the expression  $\mathcal{R}$  for the expression  $2D$  in (10).

Assume that identical copies of the example codec outlined in Section III-C are used on all MS-to-BS links in a fully loaded version of the Manhattan network in Fig. 7. The ALSE for the

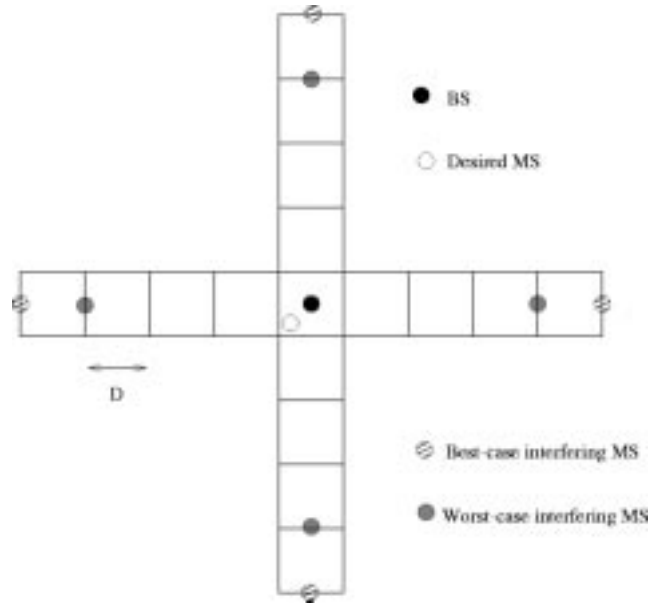


Fig. 8. Worst and best case cochannel interference configurations. All worst case interfering MSs are in distance  $4D - D/2$  from the BS, while the distance between the BS and best case interfering MSs is  $4D + D/2$ .

MS-to-BS links is plotted in Fig. 9 for the worst case interference configuration. When  $r = 20$  and  $D = 1000$ , the ALSE has a value of 8.5; for  $r = 200$  and  $D = 400$ , the ALSE is 5.2. The base-10 logarithm of the outage probability (19) is plotted in Fig. 10. A comparison of Figs. 4 and 9 and a comparison of Figs. 6 and 10 reveal that, for a given cell size, the four-cell reuse pattern results in a larger ALSE and a smaller outage probability than the two-cell reuse pattern for the worst case interference configuration. We have found that the same is true for the best case interference configuration. This is as we should expect since cochannel interference is better combatted by means of the path loss with the four-cell reuse pattern than with the two-cell reuse pattern.

#### IV. ADAPTIVE VERSUS NONADAPTIVE CODING SCHEME

A large number of trellis codes constructed especially for fading channels are described in the literature [43], [44, ch. 10]. Many of these trellis codes are designed to be decoded with the Viterbi algorithm. Consequently, the decoding of an information bit is based on a relatively short sequence of received channel symbols compared to the number of symbols utilized during iterative decoding of turbo codes [31]–[35]. We call a nonadaptive coded modulation scheme for a fading channel “traditional” if it utilizes a single trellis code together with Viterbi decoding.

##### A. Spectral Efficiency

In this section, we investigate how the cell length  $D$  and the distance  $r$  between the desired MS and its BS, as well as the Nakagami parameter  $m$  for the desired MS and the Nakagami parameter  $m_I$  for the interfering MSs, influence the received CIR. The obtained results are used to explain why the *average* spectral efficiency of the adaptive coded modulation scheme is larger than the *fixed* spectral efficiency of a traditional (nonadaptive) coded modulation scheme.

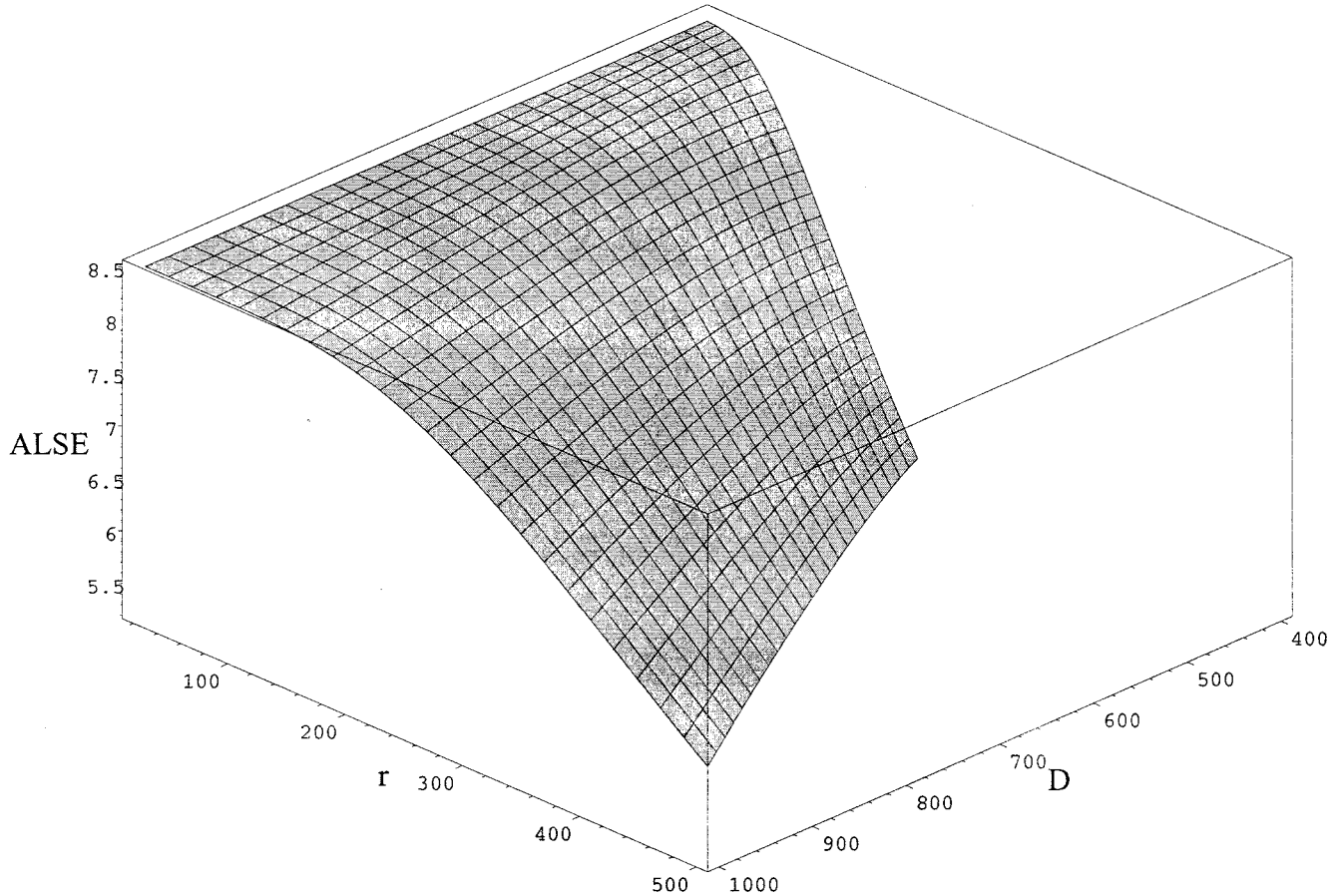


Fig. 9. ALSE [bits/s/Hz] as a function of  $D$  [m] and  $r$  [m], where  $D$  is the length of the square cells and  $r$  is the distance between the desired MS and its BS. (Fully loaded network; four-cell reuse pattern; worst-case interference configuration; target  $\text{BER}_0 = 10^{-3}$ ; two-slope path loss parameters:  $c = d = 2$ ,  $g = 240.3$ ; Nakagami parameters  $m = m_I = 2$ ; standard deviation of shadowed power mean  $\sigma_\Omega = 4$  dB; code dimension  $2L = 4$ .)

In Fig. 3, we plotted the mean of the instantaneous received CIR as a function of the distance parameters  $D$  and  $r$ . The Nakagami parameters were given values  $m = m_I = 2$ . We now study the influence of Nakagami parameters on the CIR mean. Assume that  $m, m_I \in \{2, 4, 6\}$ . The influence of  $m$  and  $m_I$  is determined by three of the terms on the right-hand side of (10)

$$\begin{aligned} \Phi(m, m_I) = & \frac{\xi}{2} \ln \left( \frac{3 + e^{\sigma_I^2/\xi^2}}{4} \right) \\ & + \xi \left[ \psi(m) - \psi(m_I) - \ln \left( \frac{m}{m_I} \right) \right] - \frac{\sigma_I^2}{2\xi} \text{ [dB]} \end{aligned}$$

where, from (6),  $\sigma_I^2 = \xi^2 \zeta(2, m_I) + \sigma_\Omega^2$  [dB]. Note that  $\Phi(m, m_I)$  is independent of the distance parameters  $D$  and  $r$ .

As an example, assume that  $\sigma_\Omega = 4$  dB. If we set  $m = 2$  and vary  $m_I$ , we get the  $\Phi(m, m_I)$  values listed in the upper half of Table II. The difference between the largest and smallest value is only  $\Phi(2, 2) - \Phi(2, 6) = 0.24$  dB. When we set  $m = 6$  and vary  $m_I$ , we obtain the  $\Phi(m, m_I)$  values in the lower half of Table II. In this case, the difference is 0.23 dB between the largest and smallest value. Consequently, the value of  $m_I$  has only a very modest influence on the CIR mean for a fixed value

of  $m$ . Similarly, it can be seen that the value of  $m$  has a somewhat larger influence on the CIR mean than  $m_I$ , but the influence is still modest.

The influence of the distance parameters  $D$  and  $r$  on the CIR mean is given by the first term on the right-hand side of (10)

$$\Theta(D, r) = \xi \ln \left( \left[ \frac{\mathcal{R} \mp D/2}{r} \right]^c \left[ \frac{g + \mathcal{R} \mp D/2}{g + r} \right]^d \right) \text{ [dB]}$$

where  $\mathcal{R}$  has been substituted for  $2D$ . Observe that  $\Theta(D, r)$  is independent of the Nakagami parameters. However, the value of the term depends on the two-slope path-loss parameters  $c$ ,  $d$ , and  $g$ . Let  $c = d = 2$  and  $g = 240.3$ . For the two-cell reuse pattern ( $\mathcal{R} = 2D$ ) and the worst case interference configuration, we obtain the difference  $\Theta(1000, 20) - \Theta(400, 200) = 38.8$  dB. We have  $\Theta(1000, 20) - \Theta(400, 200) = 39.7$  dB for the four-cell reuse pattern ( $\mathcal{R} = 4D$ ). Large differences have also been observed for the best case interference configuration. As is to be expected, we have the following observation.

*Observation 1:* The distance parameters  $D$  and  $r$  have a large influence on the value of the CIR mean while the Nakagami parameters  $m$  and  $m_I$  have only a modest influence.

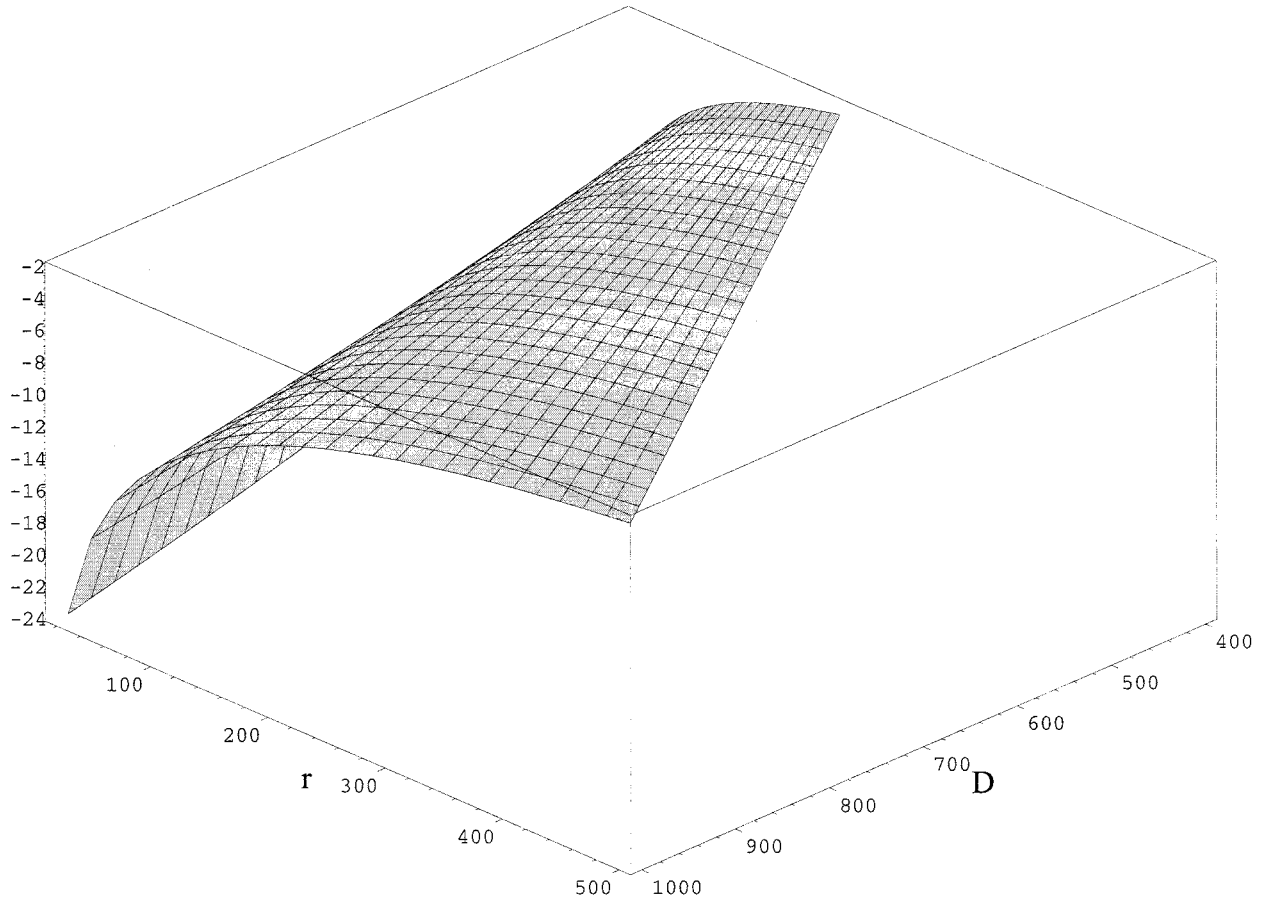


Fig. 10. Base-10 logarithm of outage probability as a function of  $D$  [m] and  $r$  [m], where  $D$  is the length of the square cells and  $r$  is the distance between the desired MS and its BS. (Fully loaded network; four-cell reuse pattern; worst case interference configuration; target  $\text{BER}_0 = 10^{-3}$ ; two-slope path loss parameters:  $c = d = 2, g = 240.3$ ; Nakagami parameters  $m = m_I = 2$ ; standard deviation of shadowed power mean  $\sigma_\Omega = 4$  dB; code dimension  $2L = 4$ .)

The CIR variance may be expressed as a function of the Nakagami parameters  $m$  and  $m_I$  by substituting the expression for  $\sigma_\gamma^2$  in (6) into (11)

$$\sigma_\gamma^2(m, m_I) = \xi^2 \left[ \zeta(2, m) + \ln \left( \frac{3 + \exp\left(\frac{\xi^2 \zeta(2, m_I) + \sigma_\Omega^2}{\xi^2}\right)}{4} \right) \right] + \sigma_\Omega^2 \text{ [dB]}.$$

Assume once more that  $\sigma_\Omega = 4$  dB. If we set  $m = 2$  and vary  $m_I$ , we get the  $\sigma_\gamma^2(m, m_I)$  values tabulated in the upper half of Table II. The difference between the largest and smallest variance value is 3.8 dB. For  $m = 6$  and varying  $m_I$ , we obtain the values in the lower half of Table II. The difference is again 3.8 dB between the largest and smallest value. Consequently, the value of  $m_I$  has a significant influence on the CIR variance for a fixed value of  $m$ . Similarly, it can be seen that  $m$  has an even larger influence on the CIR variance than  $m_I$ .

*Observation 2:* The Nakagami parameters  $m$  and  $m_I$  have a large influence on the CIR variance. The influence of  $m$  is larger than  $m_I$ .

TABLE II  
VALUES OF  $\Phi(m, m_I)$  AND  $\sigma_\gamma^2(m, m_I)$

$m$	$m_I$	$\Phi(m, m_I)$ [dB]	$\sigma_\gamma^2(m, m_I)$ [dB]
2	2	-1.47	27.5
2	4	-1.65	24.5
2	6	-1.71	23.7
6	2	-0.67	18.8
6	4	-0.85	15.7
6	6	-0.90	15.0

Let us consider a fully loaded network with reuse distance  $\mathcal{R} = 4D$  and cell length  $D = 400$ . It follows from the above discussion that the mean of the instantaneous received CIR varies greatly as the distance  $r$  between the desired MS and its BS changes. The variance of the instantaneous received CIR is largest when the Nakagami parameters  $m = m_I = 2$ . The pdf for the instantaneous received CIR is plotted in Fig. 11 for  $m = m_I = 2$  and different values of  $r$ .

*Observation 3:* Since the mean of the instantaneous CIR varies greatly as the desired MS moves around, and since the variance of the instantaneous CIR is large for severe fading, all spectrally efficient coding schemes for Manhattan networks must be able to operate over a large range of instantaneous CIR values.

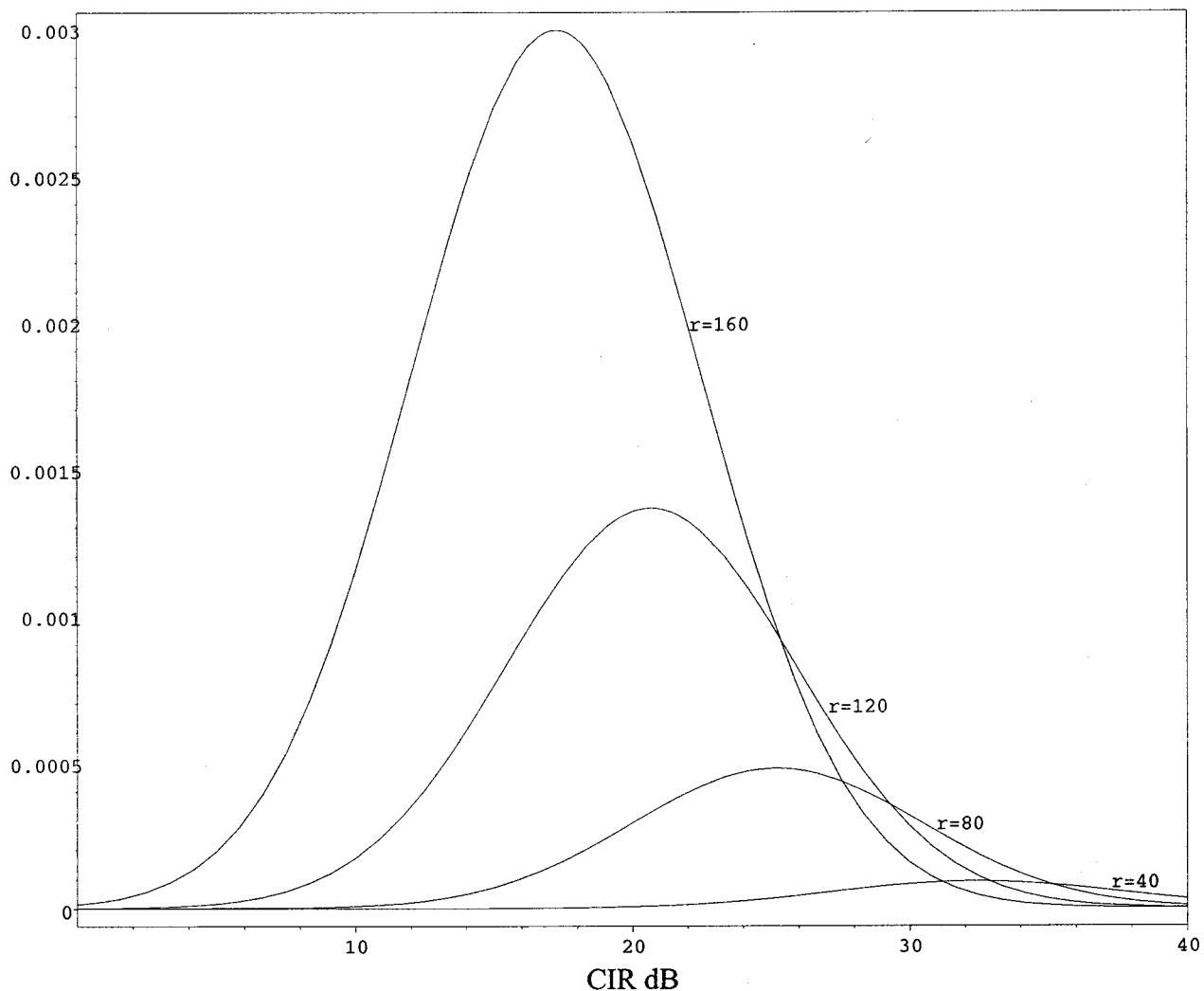


Fig. 11. PDF of instantaneous received CIR for  $r \in \{40, 80, 120, 160\}$  and  $D = 400$ . (Fully loaded network; four-cell reuse pattern; worst case interference configuration; two-slope path loss parameters:  $c = d = 2, g = 240.3$ ; Nakagami parameters  $m = m_I = 2$ ; standard deviation of shadowed power mean  $\sigma_\Omega = 4$  dB.)

Observation 3 may not be surprising; however, it follows from the observation that adaptive trellis coding can achieve a larger spectral efficiency than traditional trellis coding in urban areas. Consider a Manhattan network that utilizes a traditional coding scheme for the reverse links. Since the variance of the CIR is large when the fading is severe, the CIR may vary greatly even for a stationary MS. To use a single trellis code for a fading channel [43], [44, ch. 10], it is therefore necessary to use a code that achieves the target BER for the minimum observed CIR. This conservative design choice results in a small spectral efficiency and is the main reason why networks utilizing traditional coding schemes have spectral efficiencies less than 2 bits/s/Hz.

The general expression (14) approximating the ALSE shows that the adaptive coding scheme, based on Viterbi decoding of well-known trellis codes for AWGN channels, may achieve a much larger ALSE than the fixed spectral efficiency of traditional coding schemes based on Viterbi decoding of single trellis codes. For the example codec studied in Section III, the ALSE is no less than 5.2 bits/s/Hz (see Fig. 9) for the four-cell

reuse pattern and worst case cochannel interference configuration. This ALSE value should be reduced somewhat since we have ignored various overhead such as the introduction of pilot symbols. However, the ALSE will still be much larger than 2 bits/s/Hz.

It may be tempting to conclude from the above discussion that it is not possible to achieve a large link spectral efficiency with a single code. However, this is not true. The maximum link spectral efficiency for a given distance  $r$  between the desired MS and its BS is equal to the Shannon capacity,  $\langle C|r \rangle^\mp$  [bits/s], of the link, divided by the bandwidth  $B$  [Hz]. Assuming constant transmit power and a delay-free feedback channel, and interpreting the interfering MSs as AWGN, the maximum spectral efficiency is given by [6]

$$\frac{\langle C|r \rangle^\mp}{B} = \int_0^\infty \log_2(1 + \gamma) p(\gamma|r) d\gamma. \quad (20)$$

In (20),  $\gamma$  is the instantaneous CNR,  $B \log_2(1 + \gamma)$  is the Shannon capacity of an AWGN channel with CNR equal to  $\gamma$ ,

and  $p(\gamma|r)$  is the pdf defined in (8). The integral can be solved numerically.

There exists a theoretical adaptive coding scheme with ALSE equal to (20) [6]. What may be more surprising is that the maximum spectral efficiency (20) may also be reached without varying the information rate [45], [46]. In fact, a simple standard (Gaussian) codebook with fixed information rate will be sufficient and no feedback channel is needed, as long as the codewords are sufficiently long. Unfortunately, the decoding delay of the nonadaptive coding scheme will then be much larger than the decoding delay of the adaptive coding scheme. The reason for this is given in Section IV-B.

### B. Decoding Delay

The variable-rate coding scheme switches adaptively between  $N$  codes according to the changing value of the instantaneous received CNR  $\gamma$ . For large  $N$ , a small change in  $\gamma$  is likely to result in a change of code since the width of each fading region  $\gamma_{n+1} - \gamma_n$  is small.

A decoder is assigned to each code. Let the *initial decoding delay*  $\mathcal{D}_n$  [s] for code  $n$  be the time from the moment the decoder first receives a modulation symbol to the moment it starts decoding. The *maximum initial decoding delay* of the variable-rate coding scheme is then defined to be  $\mathcal{D} = \max_n \{\mathcal{D}_n\}$  [s]. Alternatively, the maximum initial decoding delay may be expressed in modulation symbols as

$$\Delta\mathcal{D} = \frac{\mathcal{D}}{T} = B\mathcal{D} \text{ [symbols]}$$

where  $T = 1/B$  [s].

When each code has a separate decoder, the initial decoding delay  $\mathcal{D}_n$  occurs each time the coding scheme changes code. However, in this paper, we consider sets of codes for which the same decoder may be used to decode all codes and for which it is possible to change code without interrupting decoding [8], [16]. In this case, the initial decoding delay only occurs when the communication system receives new information after a period of no transmission activity.

As long as the instantaneous CNR  $\gamma$  is (nearly) constant, the variable-rate coding scheme will utilize only one code. This period can be approximated by the channel coherence time  $T_{\text{coh}}$  [s] [28], [47], [48] or, equivalently, since it is often convenient to measure the channel coherence time in modulation symbols

$$\Delta T_{\text{coh}} = \frac{T_{\text{coh}}}{T} \text{ [symbols]}, \quad (21)$$

The system starts decoding the active code when enough noisy symbols have been received from the channel. The actual number of symbols needed to start decoding will of course depend on the active code and the decoding method. The largest possible decoding delay is obtained when the system postpones decoding the active code until a new code is activated. Consequently, the channel coherence time  $\Delta T_{\text{coh}}$  provides an approximative upper bound on the maximum initial decoding delay  $\Delta\mathcal{D}$  of the variable-rate coding scheme for large  $N$  (small fading regions). When a single codebook is utilized, the necessary length of the codebook depends on

the dynamics of the fading since the codeword length, and hence the decoding delay, must be long enough to reveal the long-term ergodic properties of the fading process. Because the instantaneous received CNR  $\gamma$  has a large variance  $\sigma_\gamma^2$ , it is clear that  $\Delta\mathcal{D} \gg \Delta T_{\text{coh}}$ .

*Observation 4:* The feedback channel enables us to reduce the maximum initial decoding delay from  $\Delta\mathcal{D} \gg \Delta T_{\text{coh}}$  down to  $\Delta\mathcal{D} \lesssim \Delta T_{\text{coh}}$  by utilizing adaptive coding instead of nonadaptive coding.

The (*total*) *decoding delay* may be defined as the sum of the initial decoding delay and the time it takes to decode a received block of noisy channel symbols. If a nonadaptive coding scheme uses an iterative decoding technique [31]–[35] to obtain a large ALSE, then the total decoding delay will also be large because the iterative decoder must operate on blocks of  $\Delta\mathcal{D} \gg \Delta T_{\text{coh}}$  symbols. An adaptive coding scheme utilizing iterative decoding may operate on blocks of  $\Delta\mathcal{D} \lesssim \Delta T_{\text{coh}}$  symbols.

### V. AVERAGE AREA SPECTRAL EFFICIENCY

We have studied the ALSE of adaptive coding schemes. For a network engineer, it may be even more interesting to consider the spectral efficiency per unit area of the network. Similarly to [27], we define and approximate the AASE. The AASE measures the efficiency of a complete network, as opposed to the ALSE, which only measures the link efficiency.

We first observe that a Manhattan network consists of identical clusters of contiguous cells where the cells in a cluster utilize different sets of carrier frequencies. A cluster of the network in Fig. 1 consists of a cell labeled A and an adjacent cell labeled B. The cluster size  $K$  of the network is  $K = 2$ . The network in Fig. 7 has  $K = 4$ .

There is a useful connection between the cluster size  $K$  and the reuse distance  $\mathcal{R}$  (defined in Section III-D). If we define the *normalized reuse distance*<sup>6</sup> as  $\mathcal{R}_n = \mathcal{R}/D$ , where  $D$  is the width of a cell, then  $K = \mathcal{R}_n$ . This can be easily checked for the two networks in Figs. 1 and 7. It is also not difficult to see that there exists a Manhattan network for any value of  $\mathcal{R}_n = K \in \{1, 2, 3, \dots\}$ . When  $\mathcal{R}_n = 1$ , then the same set of carrier frequencies is reused in every cell.

For a fully loaded network and the worst and best case interference configurations, we now define the AASE, conditioned on  $r$ , as the average information rate of all  $K \cdot U$  active MSs in a cluster divided by the product of the total bandwidth  $K \cdot U \cdot B$  utilized in, and area  $K \cdot D^2 = \mathcal{R}_n \cdot D^2$  of, the cluster

$$\begin{aligned} & \frac{K \cdot U \cdot \langle R|r \rangle^\mp}{(K \cdot U \cdot B)(K \cdot D^2)} \\ &= \frac{\langle R|r \rangle^\mp}{B \cdot (\mathcal{R}_n D^2)} \left( = \frac{\text{ALSE}}{\mathcal{R}_n D^2} \right) \text{ [bits/s]/[Hz} \cdot \text{m}^2]. \quad (22) \end{aligned}$$

The AASE defined in (22) should be thought of as the average information rate [bits/s] per unit bandwidth and area [Hz  $\cdot$  m<sup>2</sup>] associated with each BS in a cluster when all active MSs in the cluster are in distance  $r$  from their BSs and the configuration of

<sup>6</sup>Many authors define the normalized reuse distance as  $\mathcal{R}'_n = \mathcal{R}_n/(D/2)$  where  $D/2$  is the “radius” of the cell. Note that  $\mathcal{R}'_n = 2\mathcal{R}_n$ .

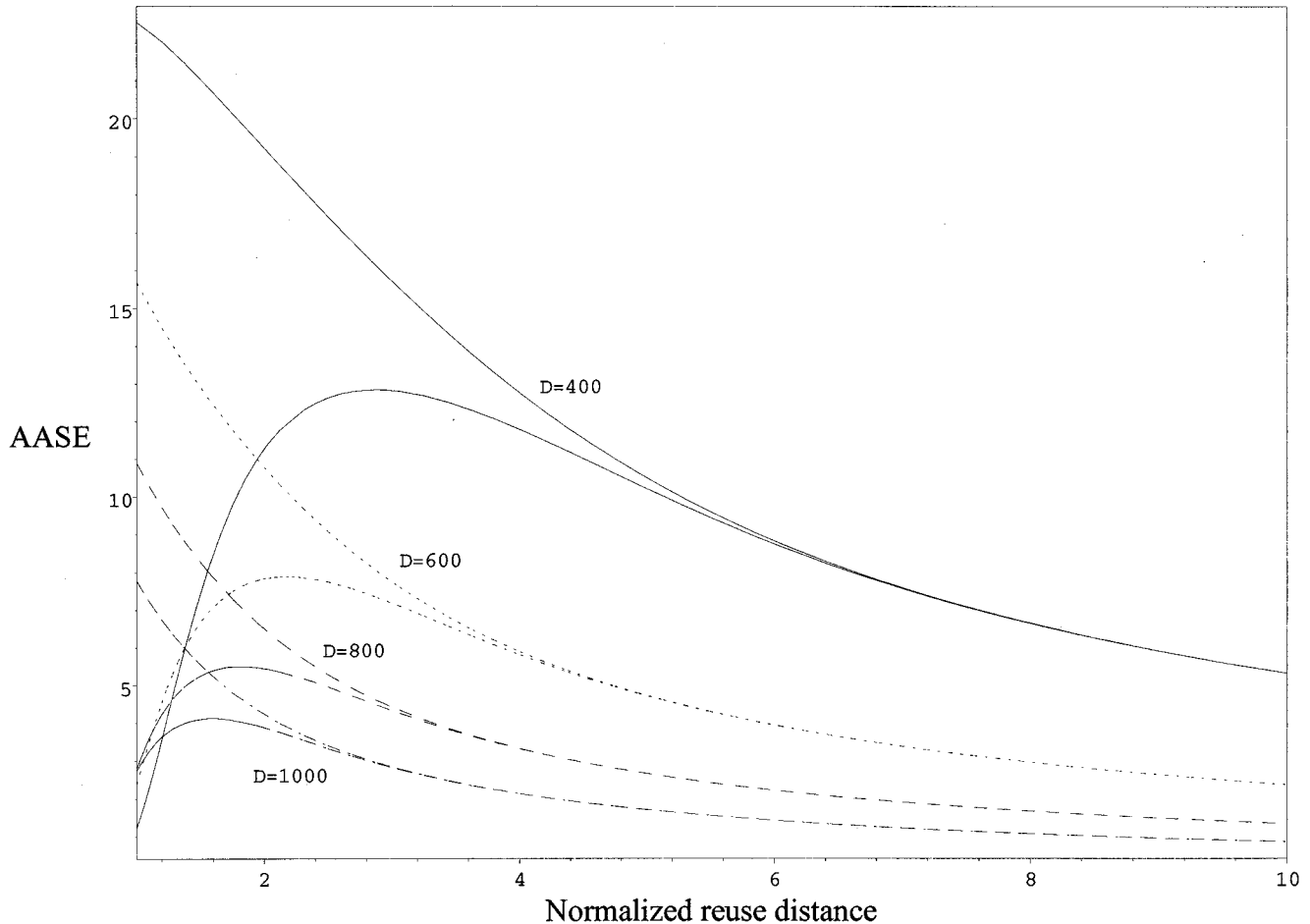


Fig. 12. AASE [bits/s/Hz/km<sup>2</sup>] as a function of the normalized reuse distance  $\mathcal{R}_n$  when  $r = 100$  and  $D \in \{400, 600, 800, 1000\}$ . (Fully loaded network; target  $\text{BER}_0 = 10^{-3}$ ; two-slope path loss parameters:  $c = d = 2$ ,  $g = 240.3$ ; Nakagami parameters  $m = m_I = 2$ ; Standard deviation of shadowed power mean  $\sigma_\Omega = 4$  dB.)

the interfering MSs outside the cluster is given by the best or worst case interference configuration.<sup>7</sup> The maximum AASE is obtained by substituting  $\langle C|r \rangle^\mp / B$  given in (20) for  $\langle R|r \rangle^\mp / B$  in (22).

The AASE of the example codec is plotted as a function of the normalized reuse distance  $\mathcal{R}_n$  in Fig. 12 for  $r = 100$ . The plot contains four pairs of curves, one pair for each value of  $D \in \{400, 600, 800, 1000\}$ . For a given pair, the upper curve is the AASE for the best case interference configuration, while the lower curve is the AASE for the worst case interference configuration. We first observe that as  $\mathcal{R}_n$  increases, the difference in AASE between the best and worst case interference configurations goes to zero. For the best case interference configuration and  $r = 100$ , the AASE decreases monotonically with increasing  $\mathcal{R}_n$ . Hence, the AASE is maximized for  $\mathcal{R}_n = 1$ , i.e., the same set of carrier frequencies is reused in every cell. The same is true for many other values of  $r$ . For the worst case interference configuration, the situation is different. For  $D = 400$ , the AASE is maximized for  $\mathcal{R}_n = 3$ , while for  $D = 1000$ , the AASE has maximum value for  $\mathcal{R}_n = 2$ .

<sup>7</sup>The expression  $\mathcal{R} = \mathcal{R}_n \cdot D$  must be substituted for  $2D$  in (10) when (22) is calculated.

To determine a good value of  $\mathcal{R}_n$  for the example codec, we again plot the AASE in Fig. 13, this time for maximum  $r = D/2$  and unchanged values of  $D$ . Note that the AASE is no longer a monotonically decreasing function for the best case interference configuration. Now, the AASE has maximum value for  $\mathcal{R}_n = 2$  when  $D \in \{600, 800, 1000\}$  and  $\mathcal{R}_n = 3$  for  $D = 400$ . Unfortunately, the difference in AASE between the best and worst case interference configurations is very large for  $\mathcal{R}_n = 2$  because the outage probability (19) is large for the worst case interference configuration [we found that  $P_{\text{out}}(\cdot) > 0.3$  for all  $D \in \{400, 600, 800, 1000\}$ ]. Hence,  $\mathcal{R}_n = 3$  is a better choice since the outage probability is significantly smaller ( $P_{\text{out}}(\cdot) < 0.06$ ). If an even smaller outage probability is needed, then  $\mathcal{R}_n = 4$  should be used ( $P_{\text{out}}(\cdot) < 0.005$ ).

## VI. SUMMARY AND CONCLUDING REMARKS

In this paper, we have modeled fully loaded microcellular radio networks for urban centers. The wireless links from the MSs to the BSs were degraded by random NMF, shadowing, and cochannel interference. The deterministic path loss associated with propagating radio waves was also incorporated in

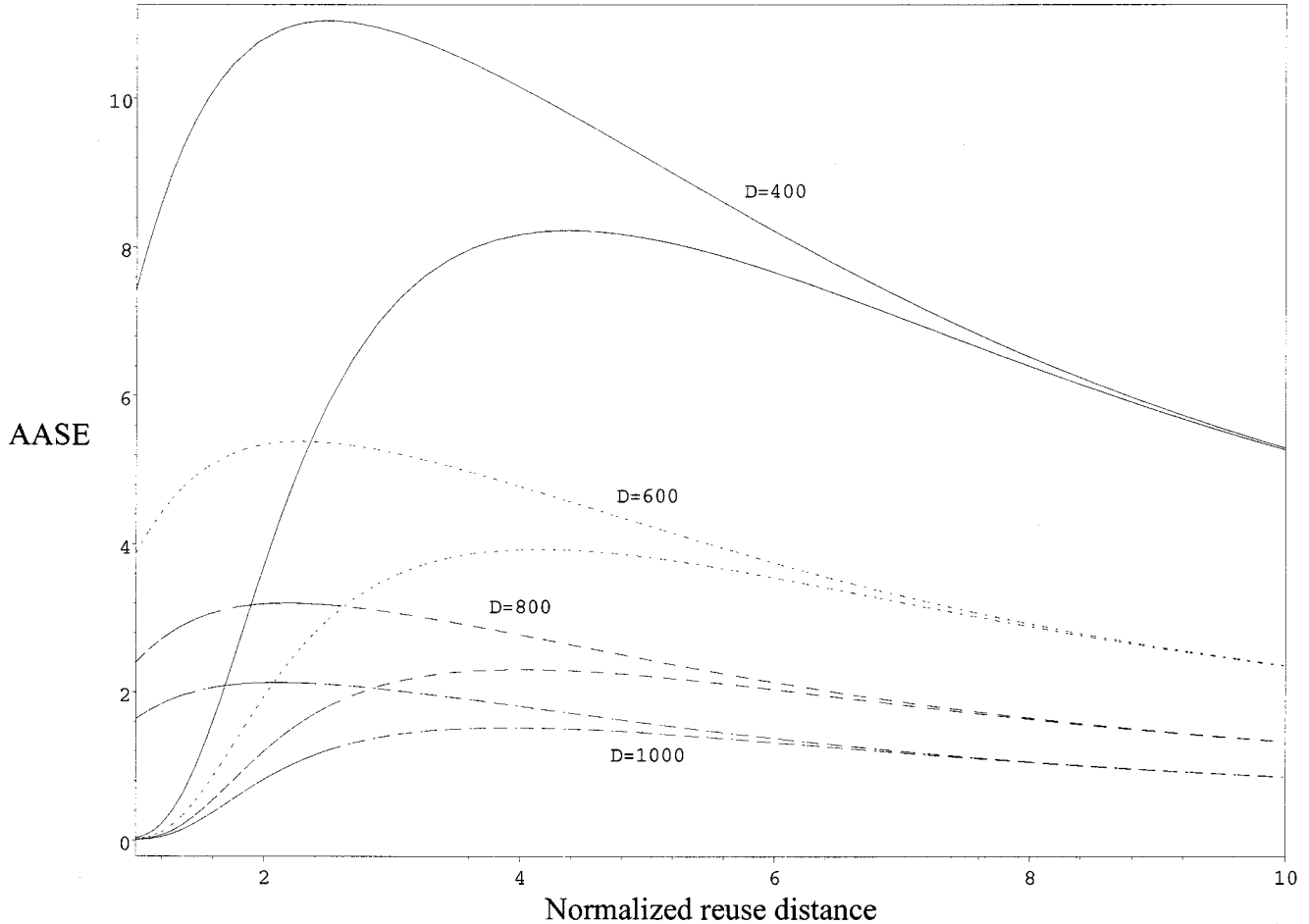


Fig. 13. AASE [bits/s/Hz/km<sup>2</sup>] as a function of the normalized reuse distance  $\mathcal{R}_n$  when  $r = D/2$  and  $D \in \{400, 600, 800, 1000\}$ . (Fully loaded network; target  $\text{BER}_0 = 10^{-3}$ ; two-slope path loss parameters:  $c = d = 2, g = 240.3$ ; Nakagami parameters  $m = m_I = 2$ ; standard deviation of shadowed power mean  $\sigma_\Omega = 4$  dB.)

the model. We outlined a general adaptive coded modulation scheme that can utilize any set of trellis codes originally designed for AWGN channels and indicated how the coding scheme fits into the network model. For the worst and best case cochannel interference configurations, we showed how to approximate the ALSE when the same instance of the general coding scheme is used on all MS-to-BS links. Moreover, it was shown why the ALSE of adaptive coded modulation schemes is larger than the spectral efficiency of traditional fixed-rate coding schemes.

An approximation of the AASE was obtained by modifying the ALSE approximation. As an example, we studied networks where identical copies of a particular codec were used on all MS-to-BS links. The codec, which is based on the International Telecommunications Union's ITU-T V.34 modem standard, utilizes eight nested two-dimensional signal constellations containing 4, 8, 16, 32, 64, 128, 256, and 512 signal points to encode and decode eight four-dimensional trellis codes. A large AASE and a small outage probability were obtained for networks with three-cell and four-cell reuse patterns of the carrier frequencies. An adaptive codec utilizing turbo-trellis codes may obtain an even larger AASE [32]–[34].

We have only approximated the ALSE and AASE of outdoor microcellular networks for urban areas. Alouini and Goldsmith [27] have modeled microcellular networks for suburban areas and macrocellular networks for suburban and rural areas. It is not difficult to generalize our approximation techniques to the outdoor networks models in [27]. It should also be possible to generalize the approximation techniques to indoor picocellular networks [49].

#### APPENDIX

##### EVALUATION OF PROBABILITY $P_{\mp, r}(\beta, \infty)$

In the following, we calculate the integral

$$\begin{aligned}
 P_{\mp, r}(\beta, \infty) &= \int_{\beta}^{\infty} p(\gamma|r) d\gamma \\
 &= \frac{\xi}{\sigma_{\gamma}\sqrt{2\pi}} \int_{\beta}^{\infty} \frac{1}{\gamma} \\
 &\quad \cdot \exp\left(-\frac{[10\log_{10}\gamma - \mu_{\gamma, \mp}(r)]^2}{2\sigma_{\gamma}^2}\right) d\gamma, \\
 &\quad \beta \geq 0
 \end{aligned}$$

where the pdf  $p(\gamma|r)$  is defined by (8). We first introduce a new variable by the substitution

$$u = \frac{10 \log_{10} \gamma - \mu_{\gamma, \mp}(r)}{\sqrt{2} \sigma_{\gamma}}$$

to obtain the integral

$$P_{\mp, r}(\beta, \infty) = \frac{1}{\sqrt{\pi}} \int_{\chi(\beta)}^{\infty} e^{-u^2} du \quad (23)$$

for  $\chi(\beta)$  defined by (17). Next, we study the integral in (23). The lower integration limit  $\chi(\beta)$  may be both negative and positive. Assume that  $\chi(\beta) < 0$ . Since the function  $y = \exp(-x^2)$  is symmetric about the  $y$ -axis and  $\int_0^{\infty} \exp(-x^2) dx = \sqrt{\pi}/2$  [39, eq. (3.321.3), p. 354], we have

$$\begin{aligned} \int_{\chi(\beta)}^{\infty} e^{-u^2} du &= \int_{\chi(\beta)}^0 e^{-u^2} du + \int_0^{\infty} e^{-u^2} du \\ &= \int_0^{-\chi(\beta)} e^{-u^2} du + \frac{\sqrt{\pi}}{2}. \end{aligned} \quad (24)$$

For  $\chi(\beta) \geq 0$ , we write

$$\begin{aligned} \int_{\chi(\beta)}^{\infty} e^{-u^2} du &= \int_0^{\infty} e^{-u^2} du - \int_0^{\chi(\beta)} e^{-u^2} du \\ &= - \int_0^{\chi(\beta)} e^{-u^2} du + \frac{\sqrt{\pi}}{2}. \end{aligned} \quad (25)$$

Using (15), (24) and (25) may be combined to obtain

$$\int_{\chi(\beta)}^{\infty} e^{-u^2} du = \operatorname{sgn}(-\chi(\beta)) \int_0^{|\chi(\beta)|} e^{-u^2} du + \frac{\sqrt{\pi}}{2}. \quad (26)$$

Substituting (26) in (23) and using (16), we obtain

$$P_{\mp, r}(\beta, \infty) = \frac{\operatorname{sgn}(-\chi(\beta)) \cdot \operatorname{erf}(|\chi(\beta)|) + 1}{2}.$$

## REFERENCES

- [1] J. F. Hayes, "Adaptive feedback communications," *IEEE Trans. Commun. Technol.*, vol. COM-16, pp. 29–34, Feb. 1968.
- [2] J. K. Cavers, "Variable-rate transmission for Rayleigh fading channels," *IEEE Trans. Commun.*, vol. COM-20, pp. 15–22, Feb. 1972.
- [3] W. T. Webb and R. Steele, "Variable rate QAM for mobile radio," *IEEE Trans. Commun.*, vol. 43, pp. 2223–2230, July 1995.
- [4] M.-S. Alouini and A. J. Goldsmith, "Capacity of Nakagami multipath fading channels," in *Proc. 47th IEEE Vehicular Technology Conf. (VTC'97)*, Phoenix, AZ, May 1997, pp. 358–362.
- [5] A. J. Goldsmith and S.-G. Chua, "Variable-rate variable-power MQAM for fading channels," *IEEE Trans. Commun.*, vol. 45, pp. 1218–1230, Oct. 1997.
- [6] A. J. Goldsmith and P. P. Varaiya, "Capacity of fading channels with channel side information," *IEEE Trans. Inform. Theory*, vol. 43, pp. 1986–1992, Nov 1997.
- [7] M.-S. Alouini and A. J. Goldsmith, "Adaptive M-QAM modulation over Nakagami fading channels," in *Proc. 6th Communications Theory Mini-Conference (CTMC VI) in conjunction with IEEE Global Communications Conference (GLOBECOM'97)*, Phoenix, AZ, Nov. 1997, pp. 218–223.
- [8] A. J. Goldsmith and S.-G. Chua, "Adaptive coded modulation for fading channels," *IEEE Trans. Commun.*, vol. 46, pp. 595–602, May 1998.
- [9] V. K. N. Lau and M. D. Macleod, "Variable rate adaptive trellis coded QAM for high bandwidth efficiency applications in Rayleigh fading channels," in *Proc. 48th IEEE Vehicular Technology Conf. (VTC'98)*, Ottawa, ON, Canada, May 1998, pp. 348–351.
- [10] T. Ue, S. Sampei, N. Morinaga, and K. Hamaguchi, "Symbol rate and modulation level-controlled adaptive modulation/TDMA/TDD system for high-bit-rate wireless data transmission," *IEEE Trans. Veh. Technol.*, vol. 47, pp. 1134–1147, Nov. 1998.
- [11] M.-S. Alouini, X. Tang, and A. J. Goldsmith, "An adaptive modulation scheme for simultaneous voice and data transmission over fading channels," *IEEE J. Select. Areas Commun.*, vol. 17, pp. 837–850, May 1999.
- [12] D. L. Goeckel, "Adaptive coding for time-varying channels using outdated fading estimates," *IEEE Trans. Commun.*, vol. 47, pp. 844–855, June 1999.
- [13] X. Qiu and K. Chawla, "On the performance of adaptive modulation in cellular systems," *IEEE Trans. Commun.*, vol. 47, pp. 844–895, June 1999.
- [14] Y. M. Kim and W. C. Lindsey, "Adaptive coded-modulation in slow fading channels," *J. Commun. Networks*, vol. 1, pp. 99–110, June 1999.
- [15] J. M. Torrance and L. Hanzo, "Latency and networking aspects of adaptive modems over slow indoors Rayleigh fading channels," *IEEE Trans. Veh. Technol.*, vol. 48, pp. 1237–1251, July 1999.
- [16] K. J. Hole, H. Holm, and G. E. Øien, "Adaptive multidimensional coded modulation over flat fading channels," *IEEE J. Select. Areas Commun.*, vol. 18, pp. 1153–1158, July 2000.
- [17] G. Ungerboeck, "Channel coding with multilevel/phase signals," *IEEE Trans. Inform. Theory*, vol. IT-28, pp. 55–67, Jan. 1982.
- [18] G. D. Forney Jr., R. G. Gallager, G. R. Lang, F. M. Longstaff, and S. U. Qureshi, "Efficient modulation for band-limited channels," *IEEE J. Select. Areas Commun.*, vol. SAC-2, pp. 632–647, Sept. 1984.
- [19] G. Ungerboeck, "Trellis-coded modulation with redundant signal sets—Part I: Introduction," *IEEE Commun. Mag.*, vol. 25, pp. 5–11, Feb. 1987.
- [20] L.-F. Wei, "Trellis-coded modulation with multidimensional constellations," *IEEE Trans. Inform. Theory*, vol. IT-33, pp. 483–501, July 1987.
- [21] A. Chouly and H. Sari, "Six-dimensional trellis-coding with QAM signal sets," *IEEE Trans. Commun.*, vol. 40, pp. 24–33, Jan. 1992.
- [22] S. S. Pietrobon and D. J. Costello Jr., "Trellis coding with multidimensional QAM signal sets," *IEEE Trans. Inform. Theory*, vol. 39, pp. 325–336, Mar. 1993.
- [23] F.-Q. Wang and D. J. Costello Jr., "New rotationally invariant four-dimensional trellis codes," *IEEE Trans. Inform. Theory*, vol. 42, pp. 291–300, Jan 1996.
- [24] G. D. Forney Jr. and G. Ungerboeck, "Modulation and coding for linear Gaussian channels," *IEEE Trans. Inform. Theory*, vol. 44, pp. 2384–2415, Oct. 1998.
- [25] J. B. Andersen, T. S. Rappaport, and S. Yoshida, "Propagation measurements and models for wireless communications channels," *IEEE Commun. Mag.*, vol. 33, pp. 42–49, Jan. 1995.
- [26] L. R. Maciel and H. L. Bertoni, "Cell shape for microcellular systems in residential and commercial environments," *IEEE Trans. Veh. Technol.*, vol. 43, pp. 270–278, May 1994.
- [27] M.-S. Alouini and A. Goldsmith, "Area spectral efficiency of cellular mobile radio systems," *IEEE Trans. Veh. Technol.*, vol. 48, pp. 1047–1066, July 1999.
- [28] G. L. Stüber, *Principles of Mobile Communications*. Norwell, MA: Kluwer, 1996.
- [29] P. Harley, "Short distance attenuation measurements at 900 MHz and 1.8 GHz using low antenna heights for microcells," *IEEE J. Select. Areas Commun.*, vol. 7, pp. 5–11, Jan. 1989.
- [30] M. V. Clark, V. Erceg, and L. J. Greenstein, "Reuse efficiency in urban microcellular networks," in *Proc. IEEE Veh. Technol. Conf. VTC'96*, Atlanta, GA, Apr. 1996, pp. 421–425.
- [31] C. Berrou, A. Glavieux, and P. Thitimajshima, "Near Shannon limit error-correcting coding and decoding: Turbo codes," in *Proc. 1993 Int. Conf. Communication*, Geneva, Switzerland, May 1993, pp. 1064–1070.
- [32] S. Le Goff, A. Glavieux, and C. Berrou, "Turbo-codes and high spectral efficiency modulation," in *Proc. IEEE Int. Conf. Commun. (ICC'94)*, New Orleans, LA, May 1994, pp. 645–649.
- [33] P. Robertson and T. Wörz, "A novel bandwidth efficient coding scheme employing turbo codes," in *Proc. IEEE Int. Conf. Commun. (ICC'96)*, Dallas, TX, June 1996, pp. 962–967.
- [34] S. Benedetto, D. Divsalar, G. Montorsi, and F. Pollara, "Parallel concatenated trellis-coded modulation," in *Proc. IEEE Int. Conf. Commun. (ICC'96)*, Dallas, TX, June 1996, pp. 974–978.
- [35] C. Heegard and S.B. Wicker, *Turbo Coding*. Norwell, MA: Kluwer Academic, 1999.

- [36] S. Sampei and T. Sunaga, "Rayleigh fading compensation for QAM in land mobile radio communications," *IEEE Trans. Veh. Technol.*, vol. 42, pp. 137–147, May 1993.
- [37] X. Tang, M.-S. Alouini, and A. J. Goldsmith, "Effect of channel estimation error on M-QAM BER performance in Rayleigh fading," *IEEE Trans. Commun.*, vol. 47, pp. 1856–1864, Dec. 1999.
- [38] M. Nakagami, "The  $m$ -distribution—A general formula of intensity distribution of rapid fading," in *Statistical Methods in Radio Wave Propagation*, W. C. Hoffman, Ed. New York: Pergamon, 1960, pp. 3–36.
- [39] I. S. Gradshteyn and I. M. Ryzhik, *Table of Integrals, Series and Products*, 5th ed. San Diego, CA: Academic, 1994.
- [40] N. M. Temme, *Special Functions—An Introduction to the Classical Functions of Mathematical Physics*. New York: Wiley, 1996.
- [41] G. D. Forney Jr., L. Brown, M. V. Eyuboglu, and J. L. Moran III, "The V-34 high-speed modem standard," *IEEE Commun. Mag.*, vol. 34, pp. 28–33, Dec. 1996.
- [42] D. J. Costello Jr., J. Hagenauer, H. Imai, and S. B. Wicker, "Applications of error-control coding," *IEEE Trans. Inform. Theory*, vol. 44, pp. 2531–2560, Oct. 1998.
- [43] S. H. Jamali and T. Le-Ngoc, *Coded-Modulation Techniques for Fading Channels*. New York: Kluwer Academic, 1994.
- [44] E. Biglieri, D. Divsalar, P. J. McLane, and M. K. Simon, *Introduction to Trellis-Coded Modulation with Applications*. New York: MacMillan, 1991.
- [45] E. Biglieri, J. Proakis, and S. Shamai, "Fading channels: Information-theoretic and communications aspects," *IEEE Trans. Inform. Theory*, vol. 44, pp. 2619–2692, Oct. 1998.
- [46] G. Caire and S. Shamai, "On the capacity of some channels with channel state information," *IEEE Trans. Inform. Theory*, vol. 45, pp. 2007–2019, Sept. 1999.
- [47] R. Steele and L. Hanzo, *Mobile Radio Communications*, 2nd ed. Chichester, West Sussex, U.K.: Wiley, 1999.
- [48] T. S. Rappaport, *Wireless Communications: Principles and Practice*. Upper Saddle River, NJ: Prentice-Hall, 1996.
- [49] H. Hashemi, "The indoor radio propagation channel," *Proc. IEEE*, vol. 81, pp. 943–968, July 1993.



**Kjell J. Hole** (S'89–M'90) was born in Molde, Norway, on June 1, 1961. He received the B.Sc., M.Sc., and Ph.D. degrees in computer science from the University of Bergen, Norway, in 1984, 1987, and 1991, respectively.

From August 1988 to May 1990, he was a Visiting Scholar at the Center for Magnetic Recording Research, University of California, San Diego. During 1993, he was with the IBM Almaden Research Center, San Jose, CA. Since 1995, he has been a Research Scientist at the University of Bergen with funding from the Norwegian Research Council. His current research interests are in the areas of coding theory and wireless communications.

**Geir E. Øien** was born in Trondheim, Norway, on December 29, 1965. He received the M.Sc. and Ph.D. degrees in electrical engineering from the Department of Telecommunications, Norwegian Institute of Technology, Norway, in 1989 and 1993, respectively.

From August 1994 to August 1996, he was an Associate Professor in signal processing at Stavanger College, Stavanger, Norway. In August 1996, he became an Associate Professor in information theory at the Department of Telecommunications, Norwegian University of Science and Technology, Trondheim, Norway. He was President of the Norwegian Signal Processing Association from 1997 to 1999. His current research interests are in the areas of information theory and wireless communications.